CHALMERS
UNIVERSITY OF TECHNOLOGY

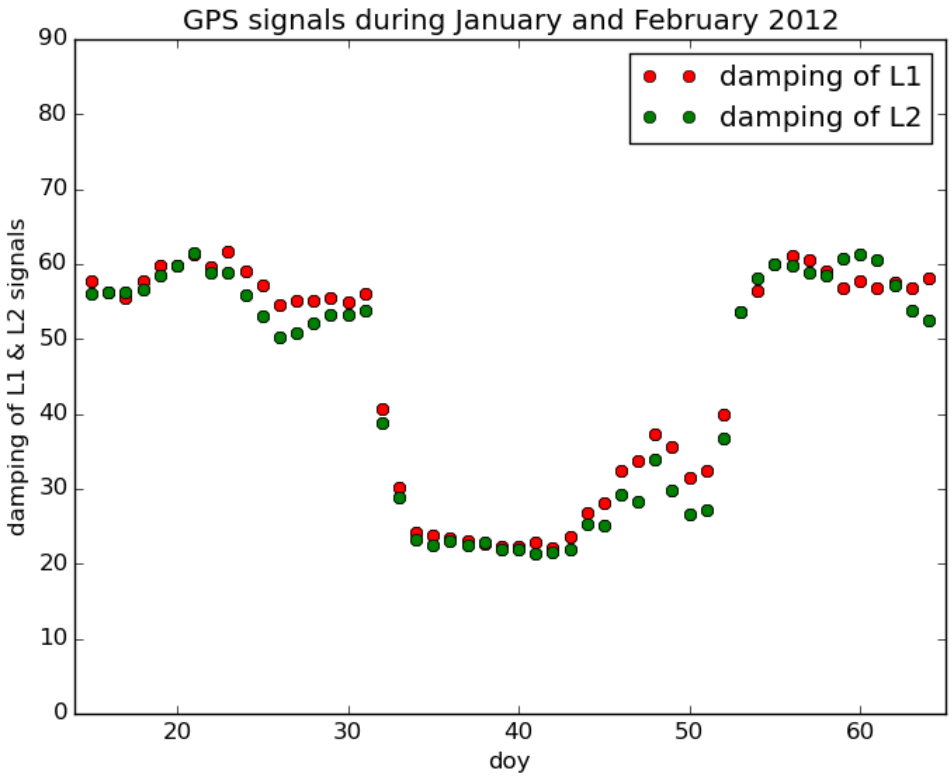

GNSS signal reflections off sea ice

Master's thesis in Wireless Photonics and Space Engineering

Eleftherios Christos Drosinos

Department of Earth and Space Sciences
CHALMERS UNIVERSITY OF TECHNOLOGY
Gothenburg, Sweden 2016

Master's thesis 2016

GNSS signal reflections off sea ice

Eleftherios Christos Drosinos

CHALMERS
UNIVERSITY OF TECHNOLOGY

Department of Earth and Space Sciences
Space Geodesy and Geodynamics
Chalmers University of Technology
Gothenburg, Sweden 2016

Supervisor: Thomas Hobiger, Associate Professor, Space Geodesy and Geodynamics, Department of Earth and Space Sciences
Examiner: Thomas Hobiger

Master's Thesis 2016
Department of Earth and Space Sciences
Space Geodesy and Geodynamics
Chalmers University of Technology
SE-412 96 Gothenburg
Telephone +46 31 772 1000

Cover: Damping of GPS L1 and L2 signals recorded at Onsala's GNSS tide gauge during January and February 2012. The decrease in the damping justifies the existence of ice on the sea surface.

Typeset in LaTeX
Printed by [Name of printing company]
Gothenburg, Sweden 2016

"An unexamined life is not worth living."

Socrates (from his speech, given at his trial, in 399 BC in Athens)

GNSS signal reflections off sea ice
Eleftherios Christos Drosinos
Department of Earth and Space Sciences
Chalmers University of Technology

Abstract

Multipath has a deleterious effect on GNSS positioning applications, but on the other hand is extremely beneficial to reflectometry, a field of science that is of utmost importance nowadays. Using GPS and/or GLONASS signals for low elevation angles, one can take advantage of this effect. Direct and reflected GNSS signals interfere with each other to form multipath signals, the composite SNR of which is recorded by a GNSS antenna connected to a receiver. While the satellites move across the sky, an interference pattern can be observed, which for low elevation angles can be very useful and one can calculate the reflector's height (distance between the antenna phase centre and the reflection surface). In this thesis, the SNR analysis technique was used to isolate the amplitude and the damping factor of dSNR in order to draw conclusions about the sea-surface conditions under freeze states in the vicinity of the GNSS-R station installed in Onsala Space Observatory. It is shown that the damping factor is more sensitive to reflected signals, than the amplitude and thus can indicate whether there is ice or not near a GNSS-R tide gauge.

Keywords: GNSS, Reflectometry, GPS, GLONASS, damping, amplitude, multipath, interference.

Acknowledgements

First of all, I would like to express my sincere appreciation to my supervisor Mr. Thomas Hobiger and to Joakim Strandberg, without the help of which, this thesis would not have been possible. No matter how busy they were, they were always willing to help and solve anything that was unclear. Both their advices and guidance have been very helpful to me.

In addition, I would like to express my sincere gratitude to Chalmers University of Technology for giving me the opportunity to attend Wireless Photonics and Space Engineering Master's Programme and expand my academic horizons far beyond that I could ever imagine.

Last but not least, I want to thank my family for the support that they provide me all of these years, because without their help I would not be able to study, expand my academic horizons and become the personality I am today.

Eleftherios Christos Drosinos, Gothenburg, November 2016

Contents

List of Figures

Abbreviations

AR	Axial Ratio
CDMA	Code Division Multiple Access
CIS	Conventional Inertial reference System
CTS	Conventional Terrestrial reference System
DoY	Day of Year
ESA	European Space Agency
FDMA	Frequency Division Multiple Access
GEO	Geostationary Orbit
GLONASS	Globalnaya Navigatsionnaya Sputnikovaya Sistema
GNSS	Global Navigation Satellite System
GPS	Global Positioning System
GSO	Geosynchronous Orbit
IAG	International Association of Geodesy
IAU	International Astronomical Union
ICRF	International Celestial Reference Frame
ICRS	International Celestial Reference System
IERS	International Earth Rotation System
IGS	International GNSS Service
IRNSS	Indian Regional Navigation Satellite System
ITRF	International Terrestrial Reference Frame
ITRS	International Terrestrial Reference System
ITU	International Telecommunications Union
IUGG	International Union of Geodesy and Geophysics
JPL	Jet Propulsion Laboratory
LHCP	Left Hand Circular Polarization
MEO	Medium Earth Orbit
NASA	National Aeronautics and Space Administration
NNSS	Navy Navigation Satellite System
PARIS	Passive Reflectometry and Interferometry System
RHCP	Right Hand Circular Polarization
RINEX	Receiver Independent Exchange
SINEX	Software Independent Exchange
SNR	Signal to Noise Ratio
SoL	Safety of Life
SPS	Standard Positioning Service
TEC	Total Electron Content

Chapter 1

Introduction

It was not long ago since NASA published a study in the Journal "Science Advances" (1), where it was stated that global warming has changed the distribution of mass on Earth, which consequently has made the North Pole and the polar motion to change course. The effect of global warming will have huge consequences both on Earth and humans the next years. The impacts of the climate change on Earth (3), can be categorized as:

- Physical
- Ecological
- Social
- Abrupt and large scale changes

A more detailed description can be read in Figure 1.1. However, as mentioned above, the effects will also have a major impact on humans. Firstly, peoples' lives are already and will continue to be under threat by the continuous changes of the climate. Storms, huge waves and cyclones are threatening people everyday and have, as well, impacts on the global economy. Moreover, humans' health, both physical and mental, will be severely affected. The former, due to polluted air and water, insufficient food supplies and diseases (transmitted with water and those transmitted by insects) (4). The later, as it has been proven, forms three different classes of psychological effects (5):

- Direct (severe psychological effects due to extreme weather conditions and due to the change of the environment)
- Indirect (people become emotionally vulnerable due to their uncertainty of what the future will bring)
- Psychosocial (psychological effects on people trying to adjust their lives to new circumstances after migration, due to heat, drought etc.)

Besides the effects on humans' health, people will be forced, due to desertification and rising sea levels, to migrate to other, safer for them, places. History, however, has shown that displacement of people creates violent conflicts, international instability and is a potential threat to international security as well. All these factors mentioned above are, among all others, strong indications that Global Navigation Satellite System Reflectometry (GNSS-R) is, more than ever, of great importance nowadays.

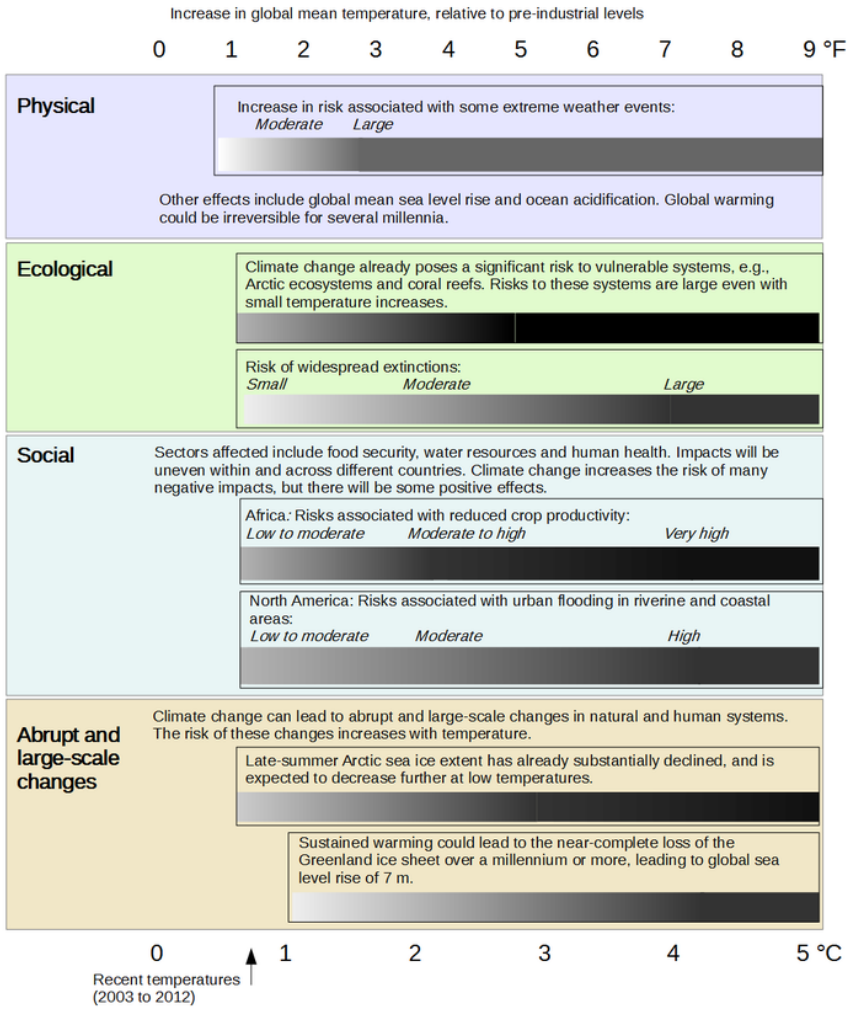

Figure 1.1: Impact of climate change. The above figure was taken from (3).

1.1 GNSS Reflectometry

By the term "Reflectometry" we define the technique that allows us to analyze the properties of a medium. It is based upon reflection of waves at the interface we want to examine. In this thesis, we study the sea area near the Onsala Space Observatory's tide gauge and try to figure out when it was covered with ice and when no ice was present.

GNSS is a revolutionary invention that started with the development of GPS and GLONASS from the United States and the Soviet Union respectively. The GPS project started in 1973 and is credited to Roger L. Easton, Ivan A. Getting and Bradford Parkinson. The first launch took place in 1978. However, the system became fully operational in 1995. Soviets began developing GLONASS in 1976. The first launch of a GLONASS satellite took place in 1982 and it also became fully operational in 1995. Both systems were initially developed for military purposes. China has also developed its own system named BeiDou Navigation Satellite System, while the European Union will have its own system, "Galileo", fully operational by

2020. India, on the other hand, recently launched its seventh and final satellite and created, this way, its own satellite navigation system, the so called Indian Regional Navigation Satellite System (IRNSS). The system consists of 7 satellites, 3 of them in geostationary orbits and 4 in geosynchronous orbits. All these systems will be discussed in Chapter 2 in more detail. GPS and GLONASS, as stated above, might initially started to be developed for military purposes, but along the way it was realised that they could be used for civilian purposes as well. So, GNSS started being used for navigation (boats, ships, airplanes, spacecrafts), as well as for surveying and mapping.

In general, what engineers care about most, are the direct signals sent from the satellite to the, ground based, receivers. Thus, multipath interference is an unwanted phenomenon. Actually, it is one of the main error sources for navigation and positioning, the two main applications offered by GNSS. However, it was, at some point, realized that the reflected signals could also be used for different purposes, such as the sea-level observation. The first to foresee this usage of the reflected signals was Manuel Martin Neira (6). He suggested that scientists should combine the direct and reflected, by the Earth's surface, signals to obtain the desired measurement. The concept was named Passive Reflectometry and Interferometry System (PARIS). This technique, proposed by Neira, was the start of GNSS Reflectometry as a field of high scientific interest.

Furthermore, James L. Garrison and Stephen J. Katzberg (7) proved that the reflected signal from a GPS satellite actually carries information about the roughness of the reflecting surface.

Recently it was shown (8) that signals reflected, off the ocean, can be detected by a low-Earth orbiting satellite and that these signals are highly correlated with independent measurements of sea winds.

It is, therefore, obvious that GNSS Reflectometry constitutes a, continuously, growing field of scientific research and is expected to deliver valuable results in the future.

1.2 Thesis Structure

This Thesis is divided into 5 Chapters. It tries to give to the reader a general idea about GNSS and GNSS-R, so that one can, later on, understand the application of GNSS Reflectometry in real life and more specifically the information acquired from signals reflected off the sea surface, as well as signals reflected off sea surface covered by ice.

Chapter 1 is an introduction trying to familiarize the reader with the concept of GNSS and GNSS Reflectometry and illustrates why the later is a field under continuous scientific research nowadays.

Chapter 2 introduces in more detail the GNSS. Principles behind GNSS are discussed, as well as the Reference Systems and Networks and the different positioning

systems that have already been operational and the ones to become operational in the near future.

Chapter 3 serves as a small introductory section before the presentation of the real data analysis that was performed with observations from the GNSS-R station in Onsala. Moreover, its goal is to give the reader a more thorough insight about what is to follow in chapter 4. Reflected GNSS signals, SNR analysis technique, as well as the characteristics of the reflecting surface are discussed.

Then, follows chapter 4 with the presentation of the results of the real data that have been extracted from the observations made at the GNSS-R station installed at the Onsala Space Observatory and were processed with the mathematical model that Joakim Strandberg developed. The analyzed data come from January - February 2012, 2013, 2014, July - August 2013 and March - April 2015.

In the fifth chapter, the conclusions of the data analysis are presented and is shown that it is possible to quantify our assumptions and apply the same procedure to different GNSS sites around the Earth.

Chapter 2

The theory behind GNSS

GNSS actually started during the 1970s as GPS and GLONASS. The former one was developed by the USA and the latter one by the Soviet Union. Both systems were designed for military purposes (as most of the technological achievements during mankind's history). We must not forget that Cold War was active those years and this must have played its role. Along the way, as discussed in the introduction, people realised that this technology could also be used for civilian purposes. This was also the start of GNSS-Reflectometry.

This chapter tries to give the reader a more concrete idea about GNSS. The basic principles are presented (i.e. GPS, GLONASS, Galileo, IRNSS and BeiDou). Moreover, the theory behind the GNSS reflected signals is analyzed in a reader-friendly way.

2.1 About GNSS

GNSS consists, as can be seen in Figure 2.1, of 3 segments: the space segment, the control segment and the ground segment (also called user segment). The space segment includes the constellation of satellites along with its inter-satellite links. Each satellite has an atomic clock and a transmitter. The control segment consists of 3 parts (9): The master control station, the monitor stations and the ground control stations. The main responsibilities of these stations can be summarised to 3 main activities: tracking, telemetry and command. The ground segment consists of the Traffic Earth stations. By the term "Earth stations" (10) we mean the user stations that give the customer the ability to communicate directly with the space segment. This segment, also called user segment can be used either for military purposes or civilian purposes.

In general, GNSS works as follows: the distance from the receiver to several satellites with known positions is measured. What is most important, is the propagation time of the signal that each satellite sends. The receiver generates a replica signal and correlates it with the signal that is sent from the satellite (this signal is dominated by noise). By doing this, it is possible to obtain the signal propagation time.

GNSS measures pseudoranges, which come from the transmitted satellite signal.

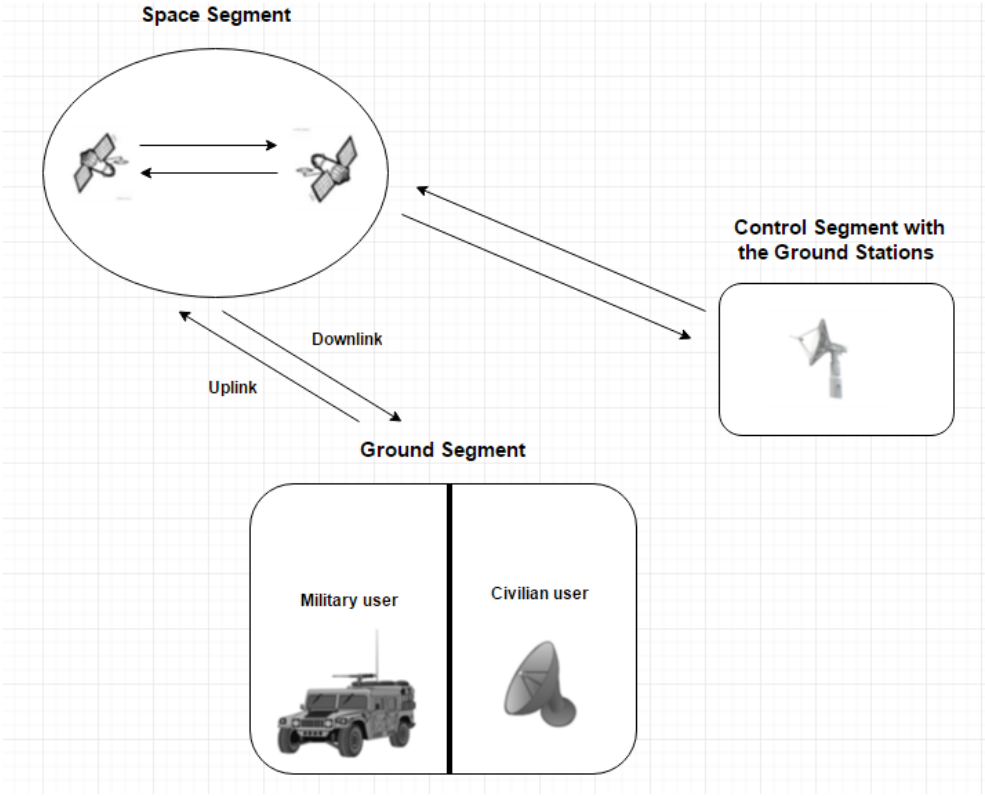

Figure 2.1: GNSS Segments.

The distance to the satellites can be measured in two different ways. The first one is to measure the time it takes for the coded signal to travel and then multiply it by its velocity and the second way is to measure the phase of the signal. In both cases, both the receiver's and the satellite's clocks are needed. The term "pseudorange" arises from the fact that these two clocks are never perfectly synchronized and thus, instead of true ranges, we get the pseudoranges, while we also take into account the clock error. A simple approach to calculate the pseudorange is the following (9):

$$R = \rho + \Delta\rho = \rho + c\delta \tag{2.1}$$

where ρ is the true range from the receiver to the satellite and $\Delta\rho$ is the range correction that results from the receiver clock error or bias δ, while c is the speed of light. From equation 2.1 it is obvious that there are four unknowns to be calculated; the three coordinates of the true receiver position plus the clock error. Thus, at least four satellites are needed to be in view every time at any location on Earth.

As we have already mentioned, each satellite sends a carrier signal. This signal contains the code and information about the satellite (the clock, the orbit, status information etc.). After this signal is correlated with the replica signal that is generated by the receiver, these components are removed. Now, it is time for the phases (phase of the carrier signal and phase of the replica signal) to be compared. This is called phase measurement. Thus, the receiver is capable to measure, the

phase difference between the received signal and the replica signal generated. In general, carrier phase measurements are more precise than the code measurements, but they contain ambiguities. However, if these ambiguities are fixed, then the carrier phase measurements can become precise at the level of a few millimeters. Since the receiver can not determine the full distance from phase measurements, since the observation is ambiguous by an integer number of wavelengths. This is called integer ambiguity. What does that practically mean? The satellite transmits a sinusoidal wave with a specific phase at the receiver. However, this signal is received by the receiver antenna with another phase. As mentioned above, the receiver generates a replica signal and correlates it to the incoming signal to perform a phase measurement. The objective problem, here, is that the integer number of wavelengths of the signal, between the satellite and the receiver, is unknown. This is what we call integer ambiguity. This can be seen in Figure 2.2.

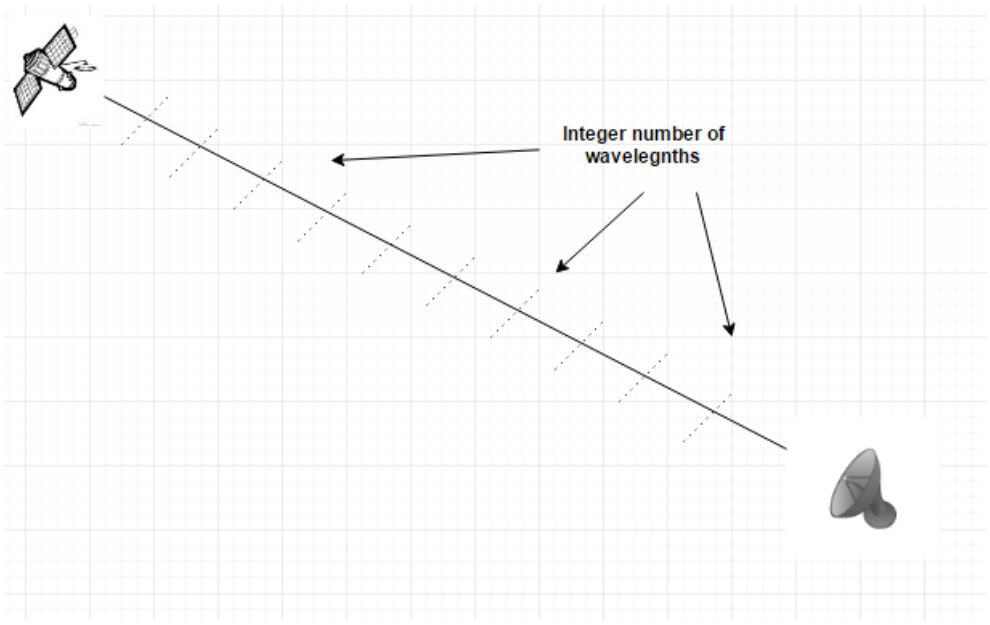

Figure 2.2: Integer ambiguity (or phase ambiguity).

The carrier phase measurement is modeled according to (9) as follows:

$$\lambda\Phi_i^j = \rho_i^j + \lambda N_i^j + c\Delta\delta_i^j - \Delta^{Iono} + \Delta^{Tropo} \tag{2.2}$$

The left side of equation 2.2 involves the multiplication of the wavelength of the carrier signal, λ and the measured carrier phase expressed in cycles. This product is, also, named as phase pseudorange. The right part of the above equation consists of the geometric distance between the observing site and the satellite, the wavelength of the carrier signal, λ multiplied by what we defined above as integer ambiguity, the speed of light in free-space multiplied by the combined clock offsets of the receiver (denoted as i) and the satellite (denoted as j), minus the ionospheric delay, plus the tropospheric delay.

The last two terms of equation 2.2 relate to the delay that the atmosphere causes to the propagation of the signals. The ionosphere, involves the upper part of the

Earth's atmosphere at an altitude of 50-1000 km. Ionosphere is mostly affected by the solar activity, since the sun is the primary source of free-electron production (ionisation of neutral atoms produces free electrons and atoms). The speed of the carrier signals when they are propagating through ionosphere depends on their electron density (12). The higher the electron density, the larger the delay of the signal. The total number of those free electrons is defined as Total Electron Density (TEC), where 1 TECU=10^{16} electrons/m^2. TEC is a function of solar activity, zenith angle, season, time of the day and magnetic latitude. However, this impact can be modeled and measured by using dual frequency observations from each satellite or by double differencing between sites that see almost the same ionosphere. Nevertheless, below an elevation angle of 15°, additional problems such as multipath, tropospheric uncertainties or separation of L1 and L2 carriers arise.

Troposphere, on the other hand, is the lowest layer of the Earth's atmosphere and extends from the surface of the Earth, up to 50 km and has approximately 75% of the atmosphere's mass. The temperature - there - decreases with increasing altitude. The effect of the tropospheric delay on the transmitted signal appears as an extra delay in the measurements. Tropospheric delay can be divided into Zenith Hydrostatic Delay (ZHD), which takes place mostly due to dry gasses that are present in the atmosphere and Zenith Wet Delay (ZWD), which is mostly due to the water vapour and weather conditions. The effect of ZHD is stronger and since the total surface pressure at mean sea level is 1013 mbar, the delay is approximately 2.3 m. The ZWD is harder to be modeled and varies - usually - between 0-40 cm (11).

2.2 Reference Systems and Networks

Reference coordinate systems are of high importance for the description of satellite motion. Also, the increasing accuracy that is being achieved by many satellite observation techniques requires a corresponding accuracy of the reference systems. In satellite geodesy, that we are interested in this thesis, the reference coordinate systems are global and geocentric (13).

2.2.1 Reference Systems

In satellite geodesy two reference systems (13) are defined:

- Space-fixed (conventional inertial reference system (CIS)) for the description of the satellites' motion.
- Earth-fixed (conventional terrestrial reference system (CTS)) for the information about the position of the receivers.

Conventional inertial reference systems are also called celestial reference systems (CRS). For the establishment of these reference systems, responsible is the International Astronomical Union (IAU). The current celestial reference system (CRS) is the International Celestial Reference System (ICRS). The origin of this system is either the barycenter of our solar system or the geocenter. The International

Celestial Reference Frame (ICRF) is a catalogue inside which the positions of 608 extragalactic radio sources are registered. These sources establish the location of the ICRS axes. More information can be found in (13).

A Conventional Terrestrial System (CTS) is defined through the Cartesian coordinates of radical stations that lie within a global network. The origin of an ideal CTS should be defined relative to the geocenter with its rotational axis (z-axis) correlating with the Earth's rotational axis (13). Unfortunately, this is not possible in real life.

In 1987, the International Earth Rotation Service (IERS) was founded by the International Astronomical Union (IAU) and the International Union of Geodesy and Geophysics (IUGG). The IERS is responsible, from 1988, for the conventional celestial and terrestrial reference systems and frames.

The current terrestrial reference system (CTS) is the International Terrestrial Reference System (ITRS). Two of its attributes are that it is geocentric and the length unit is the SI meter. The realization of ITRS is the International Terrestrial Reference Frame (ITRF). More about reference systems can be found in (13).

2.2.2 Reference Networks

Through all these years of GNSS increasing potentials, national and international reference networks have been constructed around the world. What these networks do, is to continuously record GNSS data and use them both in real-time applications or for post-processing purposes. Some of these applications include research on tectonic motion of the Earth's crust, remote sensing, etc.

2.2.2.1 International GNSS Service

The International GNSS Service (IGS) is a non-commercial federation that consists of over 200 organizations (agencies, universities, research institutions) in more than 100 countries. IGS offers open-access and high-quality GNSS data since 1994, when it was officially established by the International Association of Geodesy (IAG). IGS is controlled by the Central Bureau located at the Jet Propulsion Laboratory (JPL) in USA (9). All the organizations that belong to IGS are self-funded. IGS collects, registers (in RINEX and SINEX formats) and distributes GPS observation data sets from approximately 300 (13) distributed stations around the world with coordinates related to ITRF (9). They, also, provide high quality GNSS data, services and products in support of the international terrestrial reference system (ITRS). Some of the services that IGS provides are: Earth observations, positioning, navigation, etc. Moreover, IGS products include (14): GNSS satellite ephemerides, Earth rotation parameters, estimations on Zenith Tropospheric path delays, Global ionosphere maps, etc. In real time, predicted orbits with accuracy of about 1 m are available, while orbits that are being post-processed have a delay of two days (rapid solution) or two weeks (in case of a final solution) (9).

2.3 Global Positioning System

The GPS project started in order to substitute the TRANSIT system (also known as NAVSAT or NNSS) due to its two main disadvantages, which were the large time gaps in coverage and the low navigation accuracy (9). It was designed, primarily, for military purposes from the United States Department of Defence. GPS, in contrast to TRANSIT, is capable of measuring three variables: time, position and velocity. In section 2.1 we mentioned that, at least, four satellites are needed to be visible every time at any location from the Earth in order to have a continuous global coverage. After calculations, it was decided that GPS should have 24 satellites in 6 orbital planes with a 55° inclination and orbital period of 12 sidereal hours. The height of the satellites is 20,200 km above Earth's surface. The first satellite launch took place back in 1978 and it wasn't until 1995 that GPS was declared fully operational.

The fundamental frequency of GPS satellites is 10.23 MHz (9). By multiplying this frequency by 154 and 120 we get the L1 and L2 frequencies respectively. L1 has f= 1575.42 MHz with λ= 19.05 cm, while L2 has f= 1227.6 MHz with λ= 24.45 cm. Apart from these two frequencies, there are 2 more that are available. L3 at 1381.05 MHz available only for military users (9) and L5 at 1176.45 MHz, which will be implemented for civilian use on Block IIF satellites. It's usage will be for Safety-of-Life (SoL) applications (15).

The satellite carrier is a broad spectrum signal due to its jamming resistivity (9). Furthermore, the network of the GPS satellites uses the Code Division Multiple Access (CDMA) technique. This practically means that every satellite is assigned a unique code. In reality, each satellite is given two PseudoRandom Noise (PRN) codes. The first one is the Coarse/ Acquisition (C/A) code and is available for civilian use and is modulated upon L1 carrier. The other code is the Precision code (P-code), which, in contrast to C/A, is used for military users. Another difference between those two codes, is the fact that the P-code is modulated on both L1 and L2 carriers (9). In recent years, another civilian code modulated on the L2 carrier and is known as $L2_C$.However, apart from the PRN codes, there is also a data message that is modulated on both carriers and contains status information, satellite clock bias and satellite ephimerides (9).

2.4 Globalnaya Navigatsionnaya Sputnikovaya Sistema

GLONASS started being developed in 1976 by the Soviet Union. It is Russia's version of GPS. It provides global coverage and very good precision (5-10 m) (16). 1982 was an important year, since several satellites were lunched. However, the system became fully operational in 1995. GLONASS uses 24 satellites that are distributed in three orbital planes. The inclination of each orbital plane is 64.8°. It is clear that, since it operates at a higher inclination, GLONASS provides a higher latitude coverage than GPS that works at 55°. The height of the satellites is 19,100

km with a period of 11 h and 15 m approximately (16). As with GPS, 4 satellites are needed to get an accurate position from a receiver.

In contrast to GPS, GLONASS uses the same PRN codes for every satellite, but it uses a Frequency Division Multiple Access (FDMA) technique to distinguish between each satellite. The center frequencies are at L1 with f= 1602 MHz and λ= 18.71 cm and L2 with f= 1246 MHz and λ= 24.06 cm. The frequency ranges are calculated, for L1, according to 1602 MHz + n * 0.5625 MHz, where n is the satellite's frequency number and varies from -7 to 6 and for L2 according to 1246 MHz + n * 0.4375 MHz (9). So, the frequency ranges vary for L1 from 1598.06 MHz to 1605.38 MHz and for L2 from 1242.94 MHz to 1248.63 MHz (17).

The C/A code, which is open to civilian users, is modulated on the L1 carrier. The P code, which is also not open, is modulated on both carriers. What is also different from GPS, is the navigation message. It is transmitted by the satellites every 30 minutes and contains information about their position, velocity and acceleration vectors (9).

2.5 Galileo

Galileo is the European attempt for a global navigation satellite system, which will give Europe an independence of GPS and GLONASS. It is a project that is being developed both by the European Union and the European Space Agency (ESA). Its services will be free to everyone. In the beginning, two experimental satellites were launched in order to test the designed technologies and secure the frequencies within the International Telecommunications Union (ITU) (19). GIOVE-A in 2005 and GIOVE-B in 2008 were laucnhed (19). On October 2011 and October 2012 four satellites were launched in order to form a micrography of the 30 satellite constellation that Galileo is expected to have. Their task was to validate the system's functionality (18).

The Galileo constellation will consist of 30 satellites in three equally spaced orbital planes of 56° inclination, where each plane will have 9 satellites and 1 spare satellite. The orbits of the satellites will be circular Medium Earth Orbits (CME) and their height will be 23,222 km above Earth's surface. Their orbital period will be approximately 14 h (20).

Galileo, as GPS, uses the CDMA technique to distinguish between the satellites. It transmits in the L-band (1-2 GHz) and its signals are: E_1 with f= 1575.42 MHz and λ= 19.03 cm, E_6 with f= 1258.75 MHz and λ= 23.44 cm and E_5 with f= 1191.795 MHz and λ= 25.17 cm (21).

2.6 BeiDou

China started developing their own GNSS system, the - so-called - BeiDou. While the first BeiDou system consisted only of 3 satellites offering limited services, the

second generation, called BeiDou Navigation Satellite System (BDS) or COMPASS, is expected to have a global coverage with 35 satellites. It is, however, already operational within China with 10 satellites from 2011 (22).

The space segment of BeiDou (for global coverage) consists of 5 GEO satellites and 30 non-GEO. From those, 27 satellites will be in Medium Earth Orbit (MEO) distributed in three orbital planes at a height of 21,150 km above the Earth. Their period will be approximately 12 h 53 min with an inclination of 55.5° (17). Moreover, there will be 5 satellites in a Geostationary Earth Orbit (GEO) and 3 satellites in Inclined GeoSynchronous Orbits (IGSO) (23).

The signal bands are B_1 with carrier frequency f= 1561.098 MHz and λ= 19.217 cm, B_{1-2} with f= 1589.742 MHz and λ= 18.87 cm, B_2 with a carrier frequency of 1207.14 MHz and λ= 24.85 cm and finally B_3 with 1268.53 MHz and λ= 23.65 cm (23).

2.7 Indian Regional Navigation Satellite System

IRNSS is India's independent regional navigation satellite system. Its goal is to provide services within India, but its range covers also up to 1500 km from India's boundaries. It provides both a Standard Position Service (SPS) freely available to everyone and a Restricted Service (RS), which is available only for authorised users (24). IRNSS is already operational, since the 7th and last satellite was launched on 28th of April 2016.

It consists, as mentioned above, of 7 satellites, where 3 of them are in Geostationary Earth Orbit (GEO) at 5° inclination and 4 in Inclined GeoSynchronous Orbit (IGSO) at 29° inclination (26). Their height is approximately 36000 km above the Earth's surface (25).

IRNSS uses the L-band and the S-band for both its services (SPS and RS). It uses two carrier signals, L_5 with f= 1176.45 MHz and λ= 25.5 cm and one in S-band with f= 2492.08 MHz and λ= 12 cm.

Chapter 3

Principles behind GNSS Reflectometry

This Chapter serves as a small introductory section before the presentation of the real data analysis that was performed with data from the GNSS-R station in Onsala. Its goal is to give the reader a more thorough insight about what is to follow in chapter 4. Therefore, we will discuss, here, the principles behind the technique of GNSS Reflectometry and analyze the geometry of the system that was examined. The two basic concepts that are presented here are the **reflected GNSS signals** and the **SNR analysis technique**. Phase delay analysis will not be discussed, since only SNR analysis was used in this thesis.

3.1 Reflected GNSS Signals

It was not until recently that the reflected signals were considered as something unwanted, something that needed to be mitigated at any cost. In many applications (cell phones, GNSS tracking and positioning, etc.) the reflected signals interfere with the direct signals and create the, so called, multipath effect that affects the precision of the measurements. As we mentioned in the introduction chapter 1, Martin Neira (6) was the first to foresee the usage of the reflected signals and this, in turn, gave birth to a new scientific field called **"GNSS Reflectometry"**.

3.1.1 Advantages of Circular polarization

GNSS signals are, mostly, right hand circularly polarized (RHCP) signals. Neither vertical nor horizontal polarization is used. The reasons for this choice are quite few: circularly polarized signals are more tolerant of antenna orientation mismatches. This means that a perfect alignment between the transmitting and receiving antenna is not of critical importance. In general, we construct a circularly polarized antenna by using an horizontally polarized and a vertically polarized antenna with the outputs added with a 90° phase difference (27). However, in real life we can not have a perfectly RHCP (or LHCP) antenna. Antennas are elliptically polarized

and thus have a finite axial ratio[1] (28). Another important factor that justifies our choice for using circular polarization is the ionosphere. The ionosphere changes the signal's polarization (free electrons rotate the signal's polarization) (10). Thus, ionosphere will change the plane of polarization of a linearly polarized wave. The angle of rotation of the signal's polarization is inversely proportional to the square of its frequency. This effect is called Faraday rotation (10) and we can see that the ratio of L2 (f_2= 1227.6 MHz) over L1 (f_1= 1575.42 MHz) is 1.65 times, which means that L2 is affected more than L1. Therefore, using linear polarization for these frequencies would cause signal attenuation due to this phenomenon.

3.1.2 RHCP and LHCP signals

Whenever an RHCP satellite signal reflects off the sea surface at an angle above the Brewster angle it changes its polarization to LHCP, whereas for angles below the Brewster angle, the polarization remains unchanged, but its magnitude decreases (17). These changes can easily be seen in figure 3.1. There, we can, actually, take stock of the change in polarization of the reflected GNSS signals. Since the transmitted signal is RHCP, the co-polar and cross-polar components in the figure can be categorized as RHCP and LHCP respectively. In general, a reflected satellite signal consists of both RHCP and LHCP components due to partial polarization upon reflection from the surface (38). In figure 3.1, we see that the RHCP components' relative magnitudes are decreasing (from 1 to 0.45) for increasing angles below the Brewster angle, while the LHCP components' relative magnitudes are increasing (from 0 to 0.55) at the same time. Nevertheless, RHCP is still the dominant signal component. At the Brewster angle (from 6.5° to 10° depending on the surface) the polarization is linear, since both the amplitudes and the phases of the co- and cross-polar components are equal (this can be seen clearly for the sea water case). Above the Brewster angle, the dominant signal component is the LHCP component. In this thesis, we wanted to record GNSS signals that were reflected off both sea and sea-ice surface at low elevations and that is why we used the RHCP antenna installed in Onsala.

3.1.3 Characteristics of the Reflection Surface

So far, we have talked about the advantages of the circular polarization that is used in the GNSS signals and the change in polarization after the signal gets reflected for different angles of incidence (or elevation angles). In the following section, we will analyze the characteristics of the reflection surface.

It is obvious that the satellite signal "hits" a large area of the sea's surface (also the sea-ice's surface). Therefore, the reflection off these two surfaces can not be considered as a reflection from a single point, rather from the whole area that is being illuminated. In our case, we had two reflective surfaces to deal with. For the sea-ice surface we can assume a specular reflection (figure 3.2), since we can consider

[1] Axial ratio (AR) is defined as the ratio between the minor and the major axis of a polarization ellipse. AR for a circularly polarized antenna is unity (or 0dB).

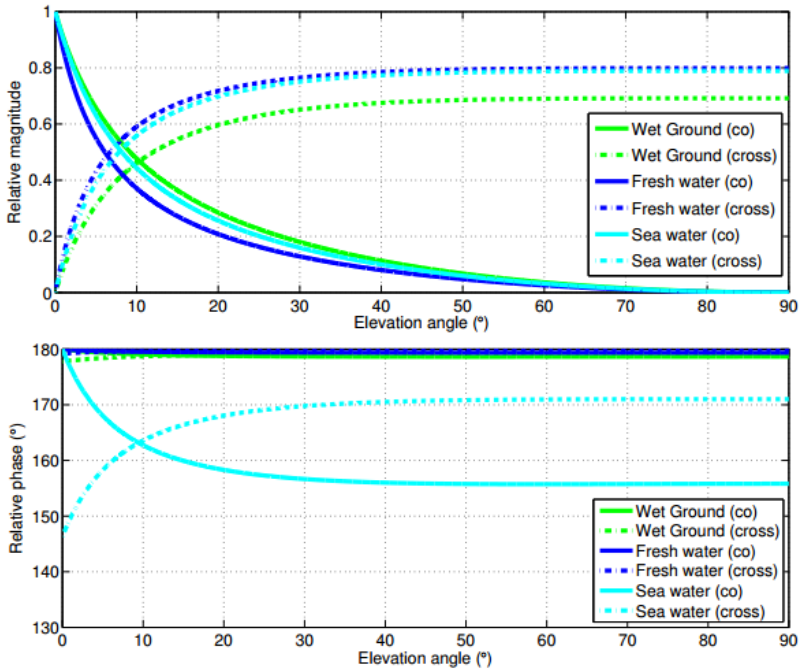

Figure 3.1: Changes in relative magnitude (top) and relative phase (bottom) of RHCP and LHCP signals after reflection off different surfaces (wet ground, fresh water and sea water) for the GPS L1 frequency. With solid line one can see the RHCP or co-polar components, while LHCP components are presented with a dashed line. This figure is taken from Figure 3.1 in (17).

this surface as a smooth one. On the other hand, for the sea surface we know that for GNSS frequencies, the Rayleigh criterion[2](44) suggests that specular reflection would be feasible only for extremely low sea roughness. When the sea surface is rough, then the reflection is diffuse[3].

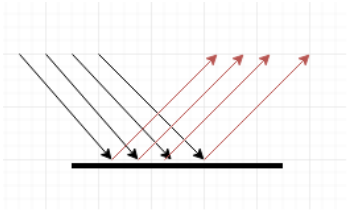

Figure 3.2: Specular reflection (smooth surface)

As we mentioned above, we have reflection areas to deal with and not just a point, since the satellite signal illuminates a large area. However, we can define the first

[2] $\Delta h < (\lambda/8)sin\theta$, where Δh is the standard deviation of the surface roughness and θ is the incident angle.

[3]For a rough surface, the incident signal is reflected at many angles and not just at one as for the specular reflection.

Fresnel zone of these areas (sea and sea-ice surface) assuming a specular surface (smooth surface, phase coherence between the signals (29), Fresnel reflection coefficient is applicable (30)). By setting the phase change δ, across the surface, equal to $\lambda/2$ (for the first Fresnel zone), we can calculate (29) the semimajor axis "a" and the semiminor axis "b" of the first Fresnel zone (which is an ellipse) to be:

$$a = \sqrt{\lambda h \sin(\gamma)}/\sin^2(\gamma) \qquad b = \sqrt{\lambda h \sin(\gamma)}/\sin(\gamma) \tag{3.1}$$

where λ is the wavelength, h is the height of the antenna (with reference to the reflector's surface) and γ is the elevation angle of the satellite (grazing angle). The first Fresnel zone can be seen in figure 3.3.

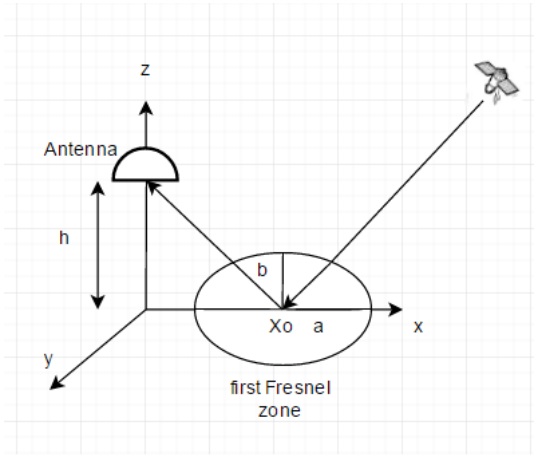

Figure 3.3: First Fresnel zone. (X_0 is the specular point)

From equation 3.1 we can see that for increasing satellite elevation angles, the reflective area (or area of the first Fresnel zone or area of the ellipse) is decreasing. For example, if we take elevation angles 10°, 30°, 50°, an antenna height of 4.3 m and λ= 19 cm, then we see that the area of the ellipse (A=πab) becomes approximately 85 m^2, 38 m^2 and 10 m^2 respectively. This means that for high elevation angles the reflective area becomes smaller and nearly circular (since a and b are almost equal).

Moreover, according to H. Davies (31) we can split the reflected signal into two parts: the coherent component of the signal and the incoherent component. Thus, a coherent wave is defined a wave of type $\exp(j\omega t + \phi)$, where the phase ϕ is constant. An incoherent wave, on the other hand, is a wave whose phase ϕ fluctuates randomly (44). The former is predominant in the case of specular reflection (see figure 3.2), where the surface reflects only coherent waves. The later starts to increase when the surface roughness increases. Taking this into account, one can be sure that above a level of sea surface roughness the receiver will not be able to detect the signal. This will occur, because the surface will scatter the satellite signal incoherently in different directions.

3.2 SNR analysis technique

The antenna that was used to receive the GNSS satellite signals in Onsala is a LEICA AR25 and its orientation is zenith looking. It is a 3D choke ring antenna. A usual choke ring antenna consists of a number of concentric conductive rings (3 to 5) around the main antenna element, called "choke rings". Their depth is approximately $\lambda/4$ (33) in order to eliminate reflected signals and prevent surface waves from propagating near the antenna (33), (32). These designs are called 2D choke ring antennas. AR25, however, is a 3D choke ring antenna. This type of antenna can track GNSS satellite signals at low elevations. AR25 can be seen in figure 3.4. More information on how this antenna works can be found in (32).

Figure 3.4: LEICA AR25 choke ring antenna.

In general, in order to reduce the multipath effect, a GNSS antenna is constructed in a way so that its radiation pattern is able to achieve high gain for the RHCP signals at elevation angles above the horizon and low gain for the LHCP signals towards negative elevation angles (or angles below the horizon) (34). From LEICA AR25's radiation pattern (Figure 3.5) we can see that the gain for the RHCP signals is maximum at the zenith (θ= 0° and el= 90°) and decreases as the elevation angles diverge from zenith. As for the LHCP signals, we can see that the gain is severely decreased compared to the gain of the RHCP signals arriving from the sky (zenith direction).

However, nothing is perfect and the, zenith looking, RHCP antenna does not completely suppress the reflected signals. Always a portion of energy, originating from signals below the horizon, reaches the antenna. The reflected signals interfere with the direct satellite signals and affect the receiver causing multipath interference (17). The signals that, finally, reach the antenna have different phases. This phase difference is responsible for the multipath interference in the receiver and as the satellite moves (following its orbit), we have an arising interference pattern. This can be seen in figure 3.6 as oscillations in the SNR (17).

When it comes to high accuracy positioning applications (road transport, aviation, telecommunications, surveying, etc) this is a problem that needs to be taken care of. But in our case (reflection off sea-ice surface) this is not something that can be considered as a problem. Actually, as Anderson (35) has already mentioned, for very

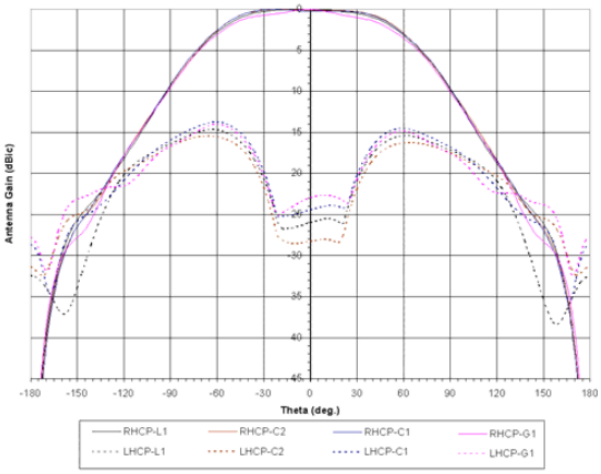

Figure 3.5: Radiation pattern of LEICA AR25.
(32)

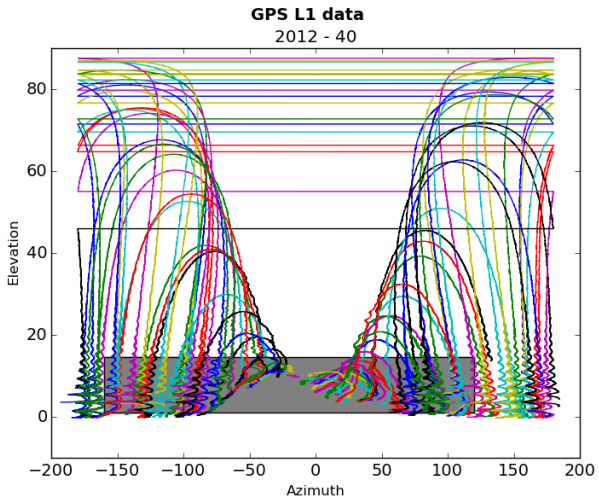

Figure 3.6: SNR oscillations for GPS L1 frequency in February 2012 (doy 40).

low elevation angles the interference pattern is influenced by atmospheric refractive effects, but for higher elevation angles these effects can be neglected and one can assume that the interference pattern is created almost because of the antenna height[4] and therefore calculate that height. Nevertheless, the methodology behind this is beyond the scope of this thesis. The reader can find more information in (35).

3.2.1 Recorded SNR and multipath frequency

In the SNR analysis method that we followed, the GNSS tide gauge looks like the schematic in figure 3.7.
Assuming a specular reflection, we can quantify the SNR (taking into account one direct and one reflected signal) as follows (36):

[4]as antenna height we define the distance between the reflection surface and the antenna phase centre.

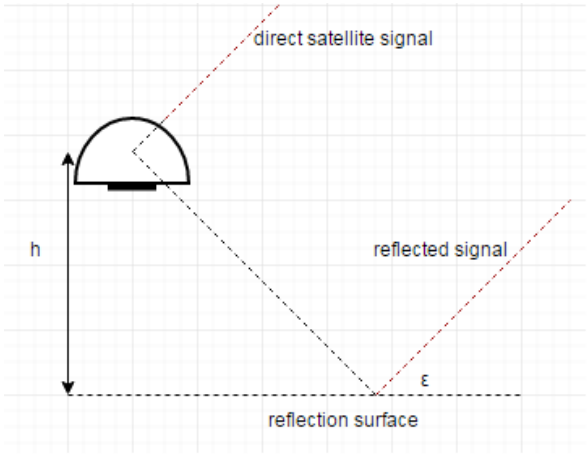

Figure 3.7: GNSS tide gauge for SNR analysis, where h is the antenna height and ϵ the elevation angle. This figure is inspired by Figure 4.3 in (17).

$$SNR^2 = A_d^2 + A_m^2 + 2A_dA_m\cos(\psi) \tag{3.2}$$

where A_m is the multipath amplitude, A_d the amplitude of the direct signal and ψ the phase difference of these two. We have already mentioned that while the satellite follows its orbit we have an arising interference pattern (seen as oscillations in the recorded SNR). Moreover, this interference pattern is dependent on the elevation angle of the satellite (multipath effects decrease with increasing elevation angle) (17), while the amplitude of the SNR oscillations depends on the surface reflectivity (36). This pattern is created, because both the reflection geometry and the phase difference change and from equation 3.2 we see that, consequently, the amplitude of the SNR changes. The frequency of these oscillations, according to (36) and for a constant reflection surface (as the sea-ice surface in our case), is calculated as:

$$\frac{\mathrm{d}\psi}{\mathrm{d}x} = \frac{4\pi h}{\lambda} \tag{3.3}$$

which indicates that the frequency is constant for a reflection surface that is not moving and is dependent on geometry of the reflecting surface and the antenna; i.e. the higher the antenna from the reflective surface, the higher the multipath frequency. But for a GNNS coastal station like the one in Onsala, a high multipath frequency and a high antenna height indicate a low sea level, while a low multipath frequency and a low antenna height indicate a high sea level. Thus, from the oscillation frequency we can, also, acquire information about the sea level.

What equation 3.2 provides us with, is the composite SNR (SNR_c= tSNR+dSNR, where the former is the trend and the latter the detrended SNR). As a consequence, we need to determine the effect that multipath has on this recorded SNR; i.e. we need to define the detrended SNR. In order to achieve this, we must isolate the multipath amplitude A_m from the direct signal's amplitude A_d. Taking into account

LEICA AR25's radiation pattern (figure 3.5) and the fact that the reflected signals reach the antenna from negative elevation angles (below horizon), we can assert that $A_d >> A_m$[5]. Therefore, by looking at equation 3.2 we see that the multipath amplitude does not affect the SNR that much. Nonetheless, the overall SNR has a large value (since A_d is large) and varies slowly during a satellite pass (17). The component of the direct signal (A_d) is usually removed with a 2nd order polynomial (37) leaving us with the multipath contribution of the SNR or the so-called detrended SNR (dSNR). This component can be modeled in accordance to (2) to be:

$$dSNR = A\sin(\frac{4\pi h}{\lambda}\sin\epsilon + \phi)\, exp(-\frac{1}{2}k^2\sin^2\epsilon) \tag{3.4}$$

where $A = 2\sqrt{P_d}\sqrt{P_r}/P_n$ is the amplitude (41) (depending on the dielectric constant of the reflecting surface, the surface roughness and the antenna gain pattern (37)), h is the antenna height, ϵ is the elevation angle and k is the wave-number.

Furthermore, if we use the Lomb-Scargle periodogram (LSP) method (39), we can calculate the height of the reflector[6]. This method (LSP) performs spectral analysis of data that are unevenly sampled (39), just like the data of the dSNR, with higher-level results, since it estimates the spectral power at each point, instead of per time interval. Thus, assuming a constant reflector (it is logical in the case of sea-ice and sea surface with low tidal ranges), we can identify the dominant oscillation frequency for each satellite pass and then convert it to reflector height (40). Depending on the result, we can obtain knowledge of the sea condition (whether it was frozen or there were any ripples).

Nonetheless, in this thesis the two important factors, from equation 3.4, that were examined were the amplitude "A" and the attenuation factor $exp(-\frac{1}{2}k^2\sin^2\epsilon)$. These two factors are of high importance, since the former is expected to be higher when the sea surface is frozen and at the same time, the latter is expected to decrease.

[5]The reader can also take a look at Figure 2 in (36).

[6]This is the distance between the phase centre of the antenna and the reflecting surface.

Chapter 4

Real data results derived from SNR method analysis

In this chapter, the real data analysis results are presented. First, there is a small introductory section with a short description of Onsala Space Observatory's GNSS tide gauge. Then, the results for sea-ice and sea surface are presented and compared. The real data analysis covers *January - February 2012 (doy 15 - doy 64) for both GPS and GLONASS signals, January - February 2013 (doy 15 - doy 47) only for GPS signals, July - August 2013 (doy 197 - doy 229) for both GPS and GLONASS signals, January - February 2014 (doy 15 - doy 64) for GPS and GLONASS signals and March - April 2015 (doy 60 - doy 91) for GPS signals.* The two factors that were of the utmost importance were the damping factor and the amplitude of the signals (see equation 3.4).

4.1 Onsala Space Observatory GNSS tide gauge

The GNSS tide gauge is located at the Onsala's Space Observatory on the Swedish west-coast (57.4° N, 11.9° E), approximately 40 km from Gothenburg. A panoramic view of the entire area around the installation can be seen in figure 4.1, while the installation can be seen in figure 4.2. However, only the zenith looking antenna (RHCP) was used in this thesis, since the analysis, as discussed in Chapter 3, was SNR-based. The receiver, a LEICA GRX1200, recorded both GPS and GLONASS signals (both L1 and L2 signals) with 1 Hz sampling rate.

The main advantage of using a single geodetic off-the-shelf GNSS receiver and the signal to noise ratio (SNR) of the satellite signals is that this method performs better in rough sea surfaces than the phase analysis method (consisting both of a zenith and nadir looking antenna) (43). It is, additionally, more tolerant and therefore more reliable during high wind speed conditions (43). As we mentioned in chapter 3, the SNR analysis method exploits the multipath interference pattern that is created from the interaction of the direct with the reflected, off the sea surface. Thus, we need to have a big reflective surface, which is also obvious from equation 3.1. It is, also, of high importance, that the reflective surface must cover as much sea area as possible, so that reflected signals from the surrounding bedrock are excluded from

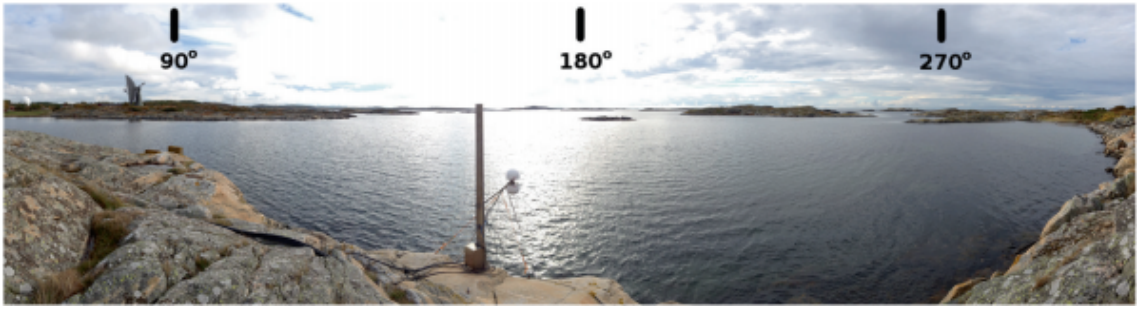

Figure 4.1: Panoramic view of the GNSS tide gauge. The figure was taken from Figure 5 in (42).

the recordings. Taking the above conclusions into consideration, it was decided that the satellite observations from elevation angles of 1° to 14.5° and azimuth angles 70° to 260° are the most valuable, since they were affected the most from the multipath effect.

Figure 4.2: Onsala's GNSS tide gauge. The figure was taken from Figure 5 in (42).

4.2 Results that indicate sea-ice conditions

The analysis of the recorded data deliberately started from February 2012, since we, already, knew that during this period there was ice in Onsala. In the following picture (Figure 4.3), taken during this time, one can, clearly, see that there is a smooth layer of ice in the area around the GNSS tide gauge installation with no snow on top of it.

Hence, according to equation 3.4, one must observe an increase in the amplitude of the signals during this period, while the damping factor should be decreased. The reason for this, is that from (44) we know that a smooth surface (as the sea-ice surface) will reflect mostly coherent waves and since the amplitude (see also section 3.2.1) is dependent on P_d^c, which is the coherent direct power of the signal and P_r^c,

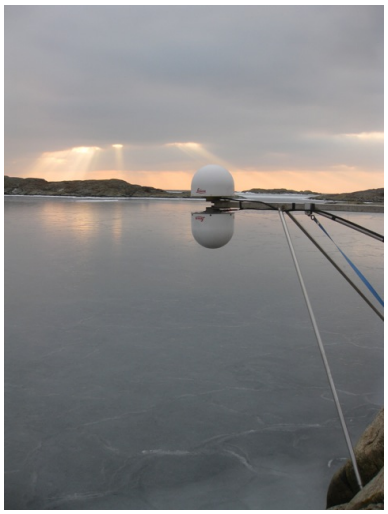

Figure 4.3: Onsala's GNSS tide gauge with ice during February 2012 (doy 37).

which is the coherent reflected power, it will be larger for the sea-ice surface, than for the open water surface.

4.2.1 January - February 2012 (doy 15 - doy 64)

In the following 4 figures (Figures 4.4, 4.5, 4.6, 4.7), the reader can see the amplitudes of L1 and L2 signals for both GPS and GLONASS satellites, as well as their damping factors. One can also refer to figures .10 and .11 in the Appendix and observe the temperature variation and the mean temperature during each day of this period.

From figure 4.4 one can observe that the amplitudes for L1 and L2 signals had, in many cases, different values. This is logical and can be explained by the fact that the two signals are transmitted with different powers, have different frequencies and so the ionosphere (Chapter 2) affects them differently.

The amplitudes showed a small increase during doy 19 - doy 20. Nonetheless, this can not be considered a satisfactory increase in the amplitude, in order to claim that the sea was frozen. The temperature (seen both in figures .10 and .11) did not indicate that either, since it remained, steadily, above 0°C. Now, on doy 32 we see a progressive increase in the amplitude, while at the same time the mean temperature was -6°C. From doy 33 - doy 36 the amplitude kept increasing with the temperature varying from -7°C to -13°C (doy 35). However, the mean temperature increased along with the amplitude, since from -12°C for doy 34 it increased to -7°C for doy 36. Then, from doy 37 - doy 40, there was a small decrease in the amplitude (from 4 to 3.8), whilst at the same time the mean temperature varied from -7°C to -5°C and decreased. From doy 41 - doy 45, the amplitudes increased again slightly.

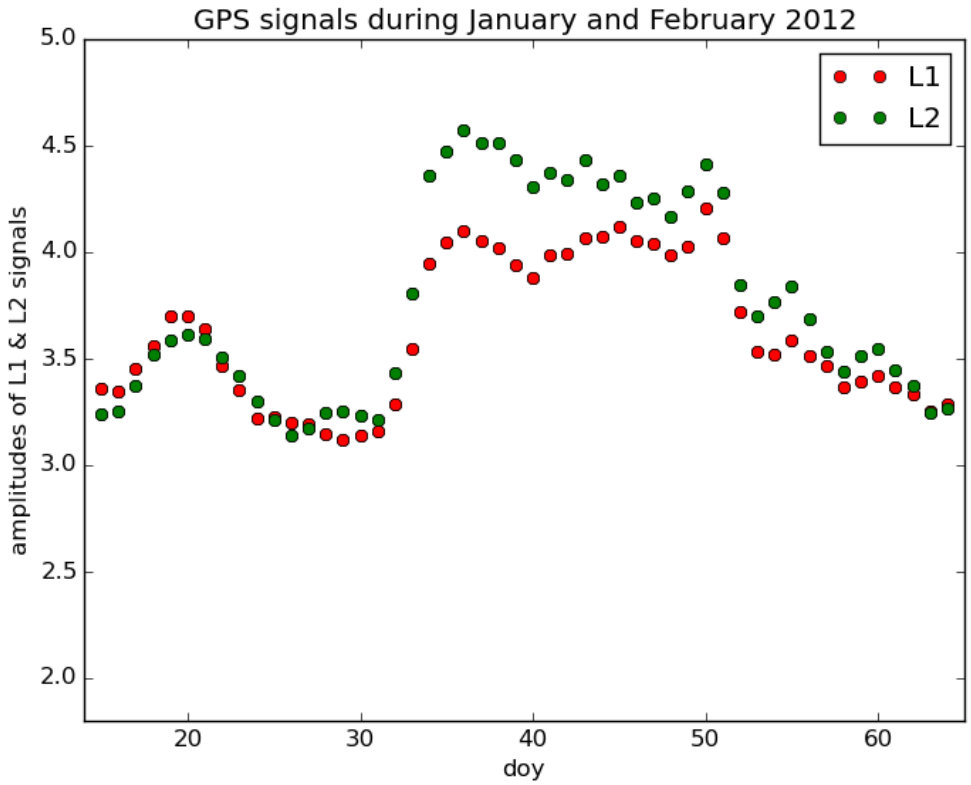

Figure 4.4: Amplitudes of GPS L1 and L2 multi-path signals

However, the temperature increased also (from -7°C (doy 41) to 0°C (doy 45)). The amplitudes decreased again from doy 46 to doy 48 and the temperature increased, from 0°C to 2°C. In doy 49 - doy 50 followed a small increase of the amplitude and finally, from doy 51 to doy 64 there was a gradual decrease in the amplitudes reaching at the same levels as for doy 30, while the temperature also increased and varied from 0°C to 5°C. From what was discussed above, it is obvious that the temperature does not have any linear relationship to the amplitudes, i.e, a possible increase in the amplitude does not require a decrease in the temperature or a decrease in the amplitude does not require an increase in the temperature. Nonetheless, the relationship between the temperature and the signals will be examined in Chapter 5. For this period of time (Jan - Feb 2012) and relying solely on the amplitudes, one could claim that the sea around Onsala's tide gauge was frozen (as can, also, be seen in figure 4.3 for doy 37) from doy 34 to doy 51. Nonetheless, as we will see by looking at figure 4.5, the damping factor is more sensitive and hence is the factor without which, we can not claim whether the sea was frozen or not. The amplitudes can - only - play an auxiliary role. For example, large values were recorded for the amplitudes, but as it will be seen in figure 4.5 some of those values correspond to days when the ice had started melting.

Looking, now, at figure 4.5 and by comparing it to the previous figure (Figure 4.4), we observe that for doy 32 and doy 33 the damping factor was decreased, whilst the

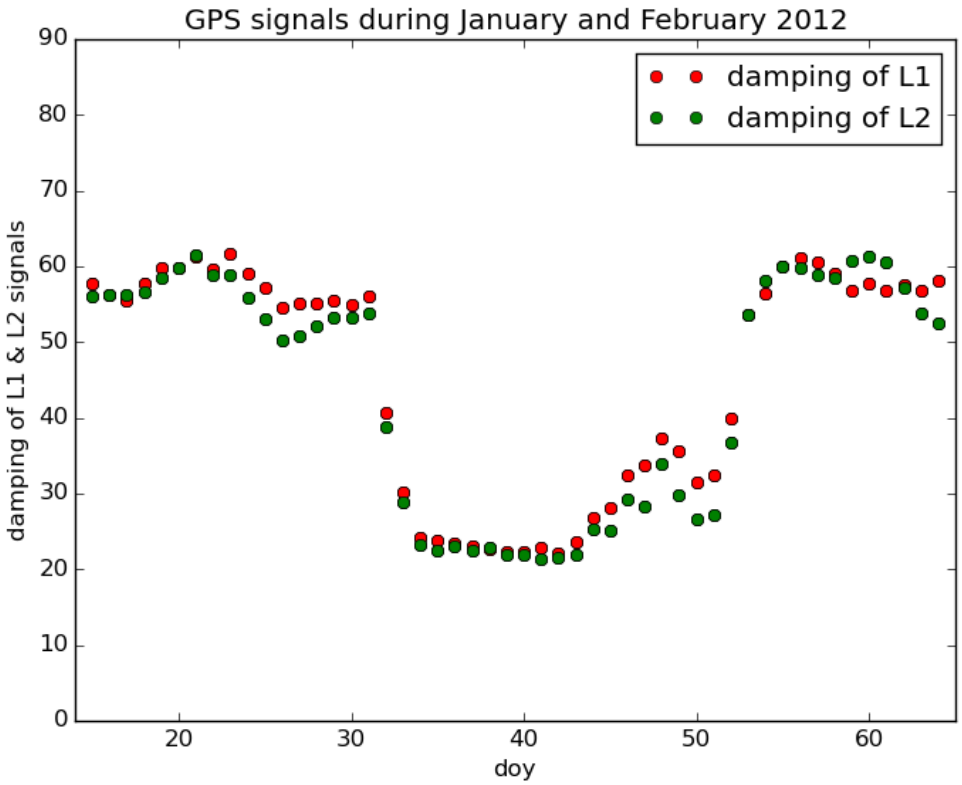

Figure 4.5: Damping factors of GPS L1 and L2 multi-path signals

mean temperature was -6°C and -7°C respectively. What is evident in this figure, is that the damping factor (for L1 signals) shows a big "gap" (approximately 15 units) from doy 31 to doy 32 and another 10 units difference from doy 32 to doy 33, whilst this is not happening for the amplitudes. This is an indication that the damping factor is more sensitive to the change of the sea surface conditions. One can say that during this period of time the sea started to freeze. Then the damping was stabilized from doy 34 - doy 43, while, on the other hand, the amplitudes had a small variation for those days. The mean temperature during this period varied from -1°C (doy 43) to -13°C (doy 35). During this time, the water around the tide gauge can be considered as frozen. Then, from doy 44 - doy 45 the ice thickness started to reduce and from doy 46 to doy 48 the damping was slightly increased, while the mean temperature was also increased from 0°C to 2°C. One can assume that the ice started melting. For doy 49 to doy 51 the damping was slightly decreased and for doy 52 started increasing with an increase in the mean temperature that was recorded to be 3°C. We can, again, observe that the transition from doy 52 to doy 53 was "clear", since the "gap" between those two days was approximately 12 units. Thus, finally, from doy 53 - doy 64 the damping factor was at the same levels as before (doy 15 - doy 31) with the mean temperature varying from 0°C to 5°C and the ice had melted.

Regarding the interference from the GLONASS satellite signals in figure 4.6, we

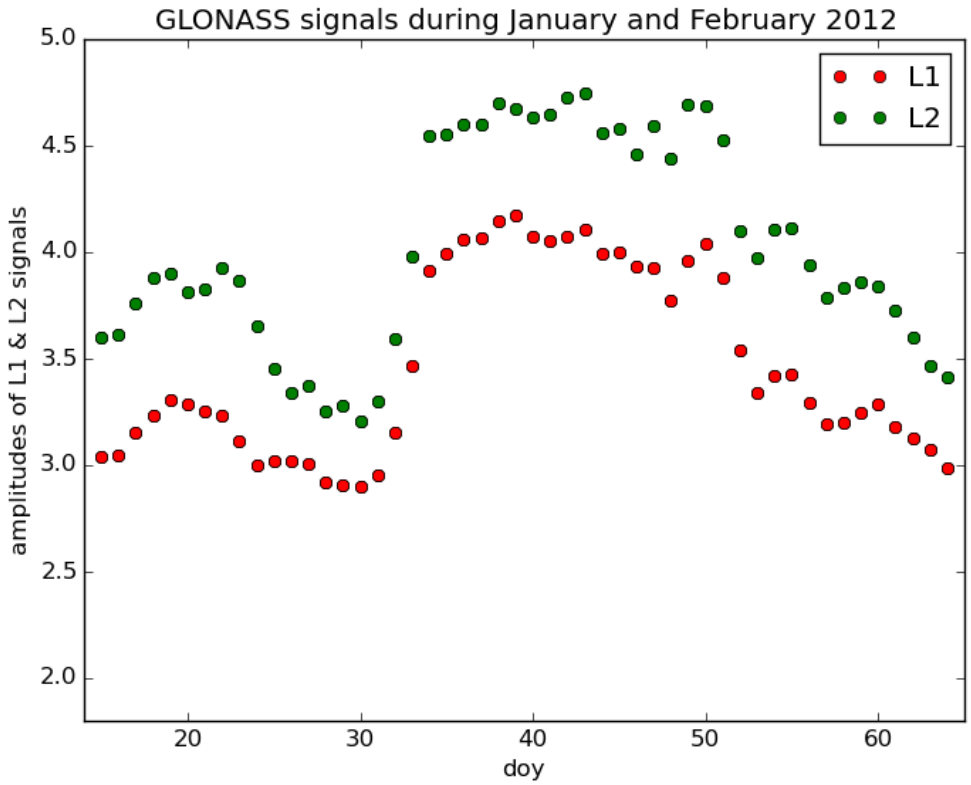

Figure 4.6: Amplitudes of GLONASS L1 and L2 multi-path signals

observe that their amplitudes followed a similar distribution as the amplitudes of L1 and L2 of the GPS satellites. We can, again, spot an increase for doy 19 and doy 20, but the level of the amplitude is, again, not satisfactory in order to be able to support that the sea was frozen. Then, there was a gradual decrease in the amplitudes with a minimum value recorded in doy 30. After that, in doy 32 there was an increase in the amplitude that continued until doy 39. From doy 40 to doy 43, the amplitudes decreased slightly and had almost the same value and from doy 44 to doy 48 a small decrease followed. During doy 49 and doy 50 there was an increase and from doy 51 the amplitudes started decreasing until doy 64, where they had the same low value as for doy 31. As we can see, the recordings of the GLONASS satellites agree, in general, with the ones we had for the GPS satellites.

In figure 4.7 we can observe the distribution of the damping factors for GLONASS L1 and L2 multi-path signals. We can see that the "gap" between doy 31 and doy 32 (for L1 signals) was approximately 13 units and between doy 32 and doy 33, around 10 units. Those differences in the value of the damping are a strong indication that the damping is, apparently, more sensitive to the sea-surface conditions. During doy 32 and doy 33 one can claim that the sea started to freeze, since the damping factor was much lower than it was for the usual sea-surface conditions (doy 15 - doy 31) and this happened due to the coherent reflections (44) that were created from the smooth sea-ice surface that started to be formed around the tide gauge. Those

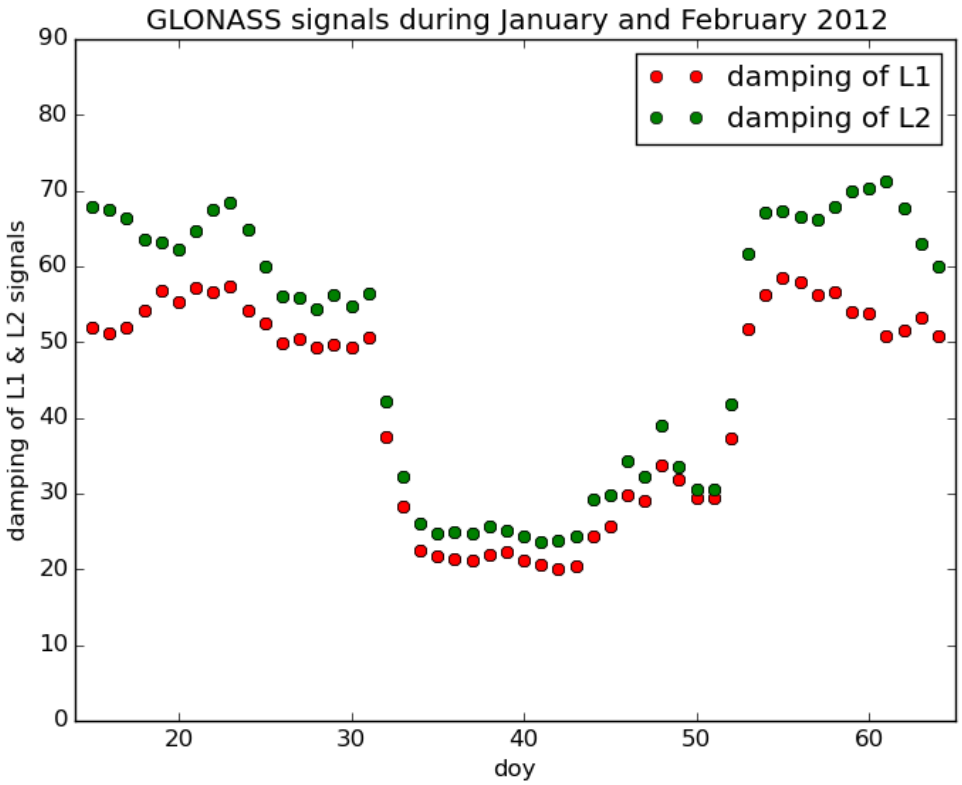

Figure 4.7: Damping factors of GLONASS L1 and L2 multi-path signals

coherent reflections increased the amplitude (see also eq. 3.4) of the signals and consequently decreased their damping (or attenuation) factor. From doy 34 to doy 43 the sea-surface was frozen and in doy 44 and doy 45 the ice started melting. This process carried on until doy 52. Then, we can see a big difference in the damping factor from doy 52 to doy 53, which is roughly 12 units. After doy 53 and until doy 64, the values of the damping factor were at the same levels as the ones for doy 15 to doy 31.

Temperature, as we already mentioned, does not have a direct relationship to the amplitude or the damping factor, but nonetheless, can give us an idea of what the weather conditions looked like. Hence, by taking a look at the figure .10 in the Appendix, one can see that the days (doy 30 to doy 33) before the "ice period" the temperature was steadily below 0°C.

4.2.2 January - February 2013 (doy 15 - doy 47)

During February 2013 and according to the analyzed data, there was also a period that the sea around the GNSS-R tide gauge in Onsala was covered by ice. Unfortunately, for this period only GPS data were available and only for doy 15 to doy 47. Thus, the following two figures (Figures 4.8 and 4.9) show the amplitudes and the damping factors of the GPS L1 and L2 multi-path signals. The amplitudes from doy

15 to doy 18 were between 3 and 3.5, lower than 4, which is a first indication[1] that there might be ice. Then, for doy 19 and doy 21 there was an increase in the amplitude and from doy 22 to doy 27 we observe an almost stable value of the amplitudes. A small increase was recorded for doy 28 and then from doy 29 to doy 32 there was a slight decrease in the amplitudes. From doy 33 to doy 35 there was a small variance in the amplitudes. Then, from doy 36 and doy 37 a gradual decrease was recorded and finally from doy 38 to doy 47 the values were at the same, approximately, levels as for doy 15 to doy 18.

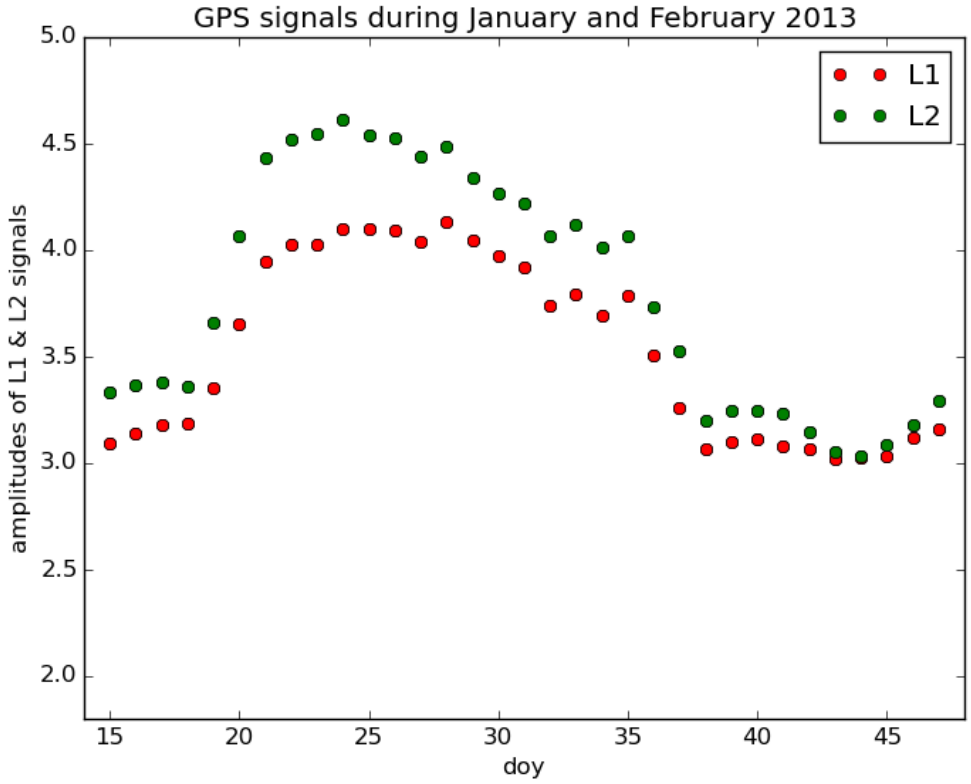

Figure 4.8: Amplitudes of GPS L1 and L2 multi-path signals

Now, by studying the damping factor for this period of time, we can draw safer conclusions about the exact time that the area was frozen. We observe in figure 4.9 that the damping factor was quite large from doy 15 to doy 18 (50 - 60) and then, for doy 19, there was a 12 units difference and another 10 units difference (roughly) for doy 20. During this time, one can claim that the area near the tide gauge started to freeze again. Then, from doy 21 to doy 28, we can affirm that the sea-surface was covered with ice, since the value of the damping factor lied between 20 and 30 units. From doy 29 to doy 32, there was an increase in the damping factor, which can be interpreted as that the ice started melting. However, one can also observe a slight decrease of the damping factor during doy 33 to doy 35. The reason for this could be that a portion of sea-ice was still present near the tide gauge. For doy 36

[1]However, as we have already said, the amplitude alone can not indicate whether there is ice or not. We need the damping factor.

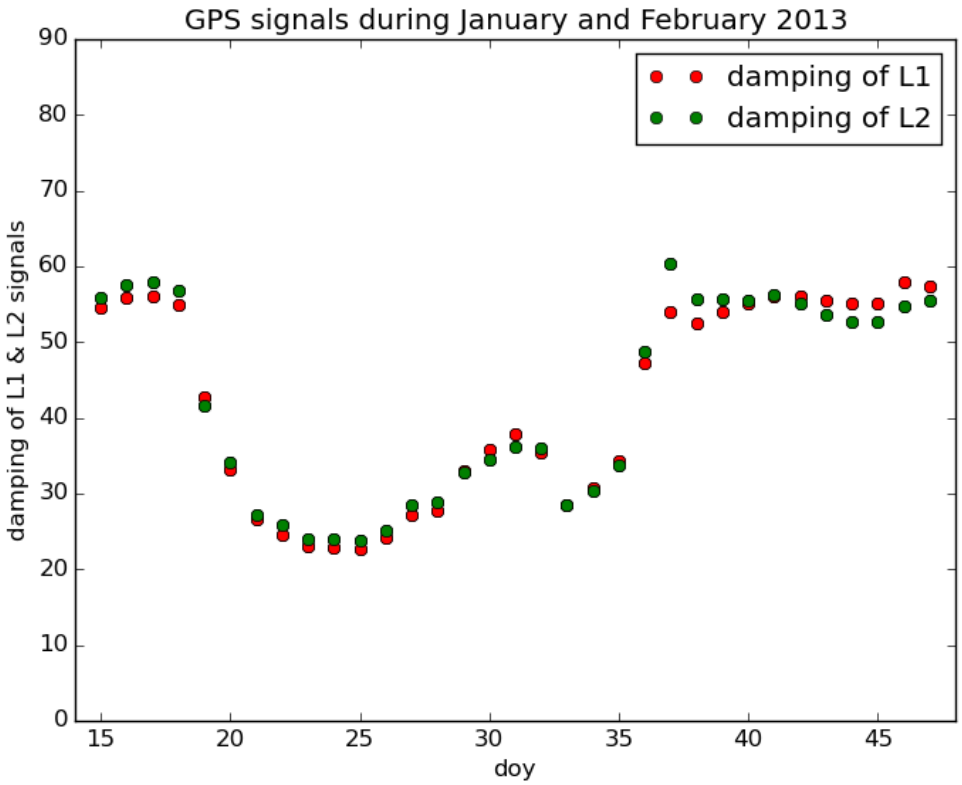

Figure 4.9: Damping factors of GPS L1 and L2 multi-path signals

there was a large increase in the damping factor, which indicates the change of the sea-surface condition, that eventually returned to its usual values from doy 37 to doy 47.

As has been said before (see Section 4.2.1), the temperature does not have any particular relationship with the amplitudes and the damping factor, but still, can provide us information about the weather conditions during the period we are looking at. For this specific period of time (Jan - Feb 2013), if we look at the figure .12 in the Appendix, we can observe that the temperature from doy 15 to doy 20 was, steadily, above 0°C and recorded a minimum of approximately -16°C for doy 20. This means that from the weather's aspect, the conditions were favorable for the ice to start being formed. Again, the relationship between the temperature and the damping will be examined in Chapter 5.

4.3 Results that do not indicate sea-ice conditions

So far (see Section 4.2), we have analyzed the derived data, from GNSS satellites, which showed that the area near the GNSS tide gauge in Onsala was frozen during the first days of February 2012 and the last days of January 2013. In this section, we will present the rest of the results that do not indicate any sea-ice conditions. Those data originate from observations done during July - August 2013 (doy 197 -

doy 229), January - February 2014 (doy 15 - doy 64) and March - April 2015 (doy 60 - doy 91).

4.3.1 January-February 2014 (doy 15 - doy 64)

For this period of time, both GPS and GLONASS data were available and therefore, in the following 4 figures (Figures 4.10, 4.11, 4.12, 4.13) one can observe the amplitudes and the damping factors of those signals. By analyzing the amplitude and damping distributions, one can ascertain, by comparing them to the results of Section 4.2, that during those days there was no ice in Onsala's GNSS tide gauge.

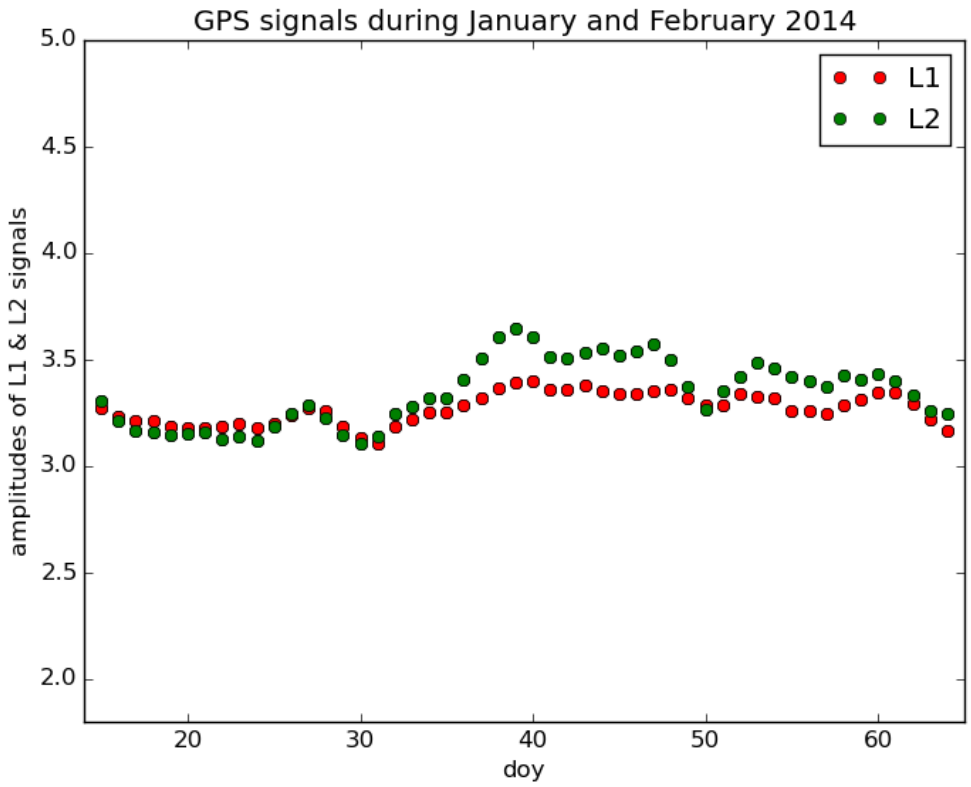

Figure 4.10: Amplitudes of GPS L1 and L2 multi-path signals

In the above figure it is obvious that the values of the amplitudes did not show any steep change during doy 15 and doy 64 as they did in Section 4.2. The largest value for the L1 amplitudes (3.4) was recorded during doy 40, while the lowest value during doy 31 (3.1). As for the L2 signals, their amplitudes took their largest value for doy 39 (3.6), whilst the lowest was recorded for doy 30 (3.1). Nevertheless, these values (the largest ones) not only are not satisfactory in order to indicate ice on the sea surface due to their low recorded amplitudes, but were also recorded only during one day for each signal, i.e. they did not show any consistency. Moreover, by looking at figure 4.4, where one can affirm the sea-ice condition, the lowest recorded value for L1 signals, during the ice period, was approximately 3.8 and for L2 signals was 4.3. Now, by looking, also, at figure 4.8, the reader can observe that the lowest

value, during the ice period, for L1 signals was approximately 3.9, whilst for L2 signals the lowest value was recorded to be 4.4. By comparing the values of the amplitudes, we can see that there is a difference of 0.4 - 0.5 for L1 signals and a difference of 0.7 - 0.8 for the L2 signals. Taking into consideration the fact that the amplitudes are not that sensitive to the sea-surface changes, the above amplitude differences provide sufficient proofs that there was no ice during doy 15 - doy 64 in 2014.
Figure 4.11 shows the damping factors of L1 and L2 multi-path satellite signals during January - February 2014. Here, one can see that the damping factors of the satellite signals vary between 50 and 60 units approximately.

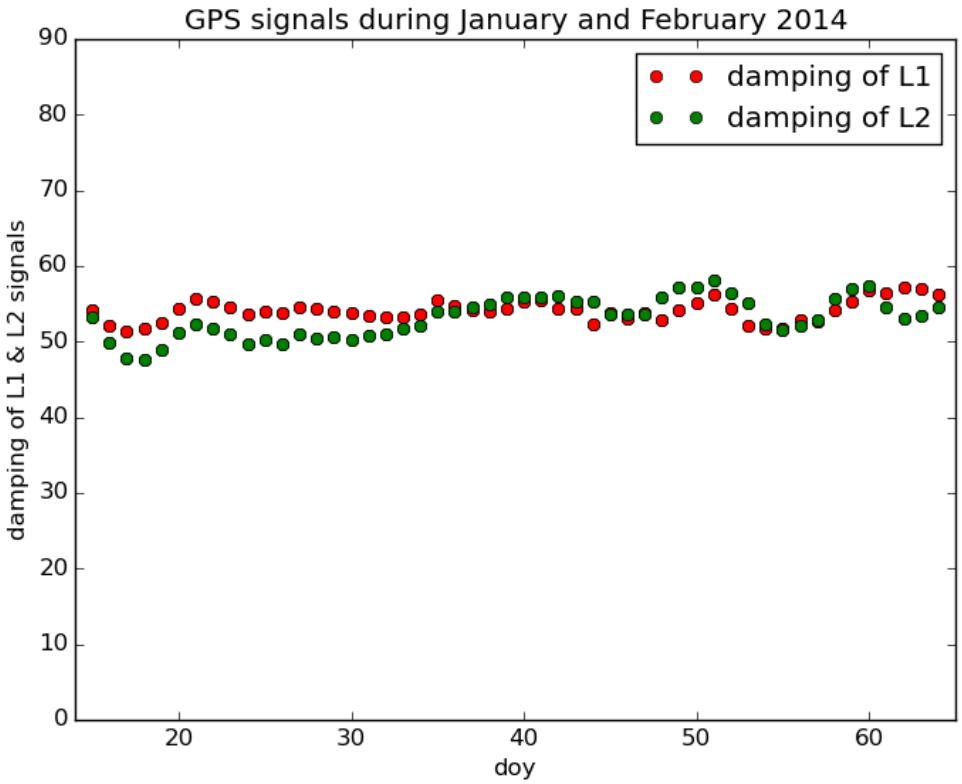

Figure 4.11: Damping factors of GPS L1 and L2 multi-path signals

However, by looking at figures 4.5 and 4.9, one can observe that in order to be in position to draw safe conclusions about whether the sea was frozen or not, the damping factors need to lie between a boundary of 20 to 28. Moreover, by comparing the above figure with these two figures, we can, certainly, see that the damping factors of L1 and L2 signals coincide with those of figures 4.5 and 4.9 for the days that the sea was not frozen. Hence, one can claim that the sea during this period was not frozen according to our GPS observations.

Now, we can study the GLONASS multi-path satellite signals by looking at figures 4.12 and 4.13. The GLONASS amplitudes observations agree, in general, with those for GPS (see figure 4.10). For the L1 signals, low values in their amplitudes were

observed from doy 15 to doy 64 and also a small variation in their values, which from doy 30 to doy 64 varied from 3.1 to 3.4 units. Nonetheless, these values were lower than the threshold value of 3.8 (for L1 signals) that we need in order to be able to claim that there might have been ice covering the sea surface. The L2 signals follow a similar variation as the L1 signals for the same period of time (doy 30 - doy 64) with recorded values between 3.1 and 3.7 approximately, while at the same time their amplitude values coincide with the values of L2 signals of the GPS satellites. Therefore, we can claim that during this period of time the sea was not frozen.

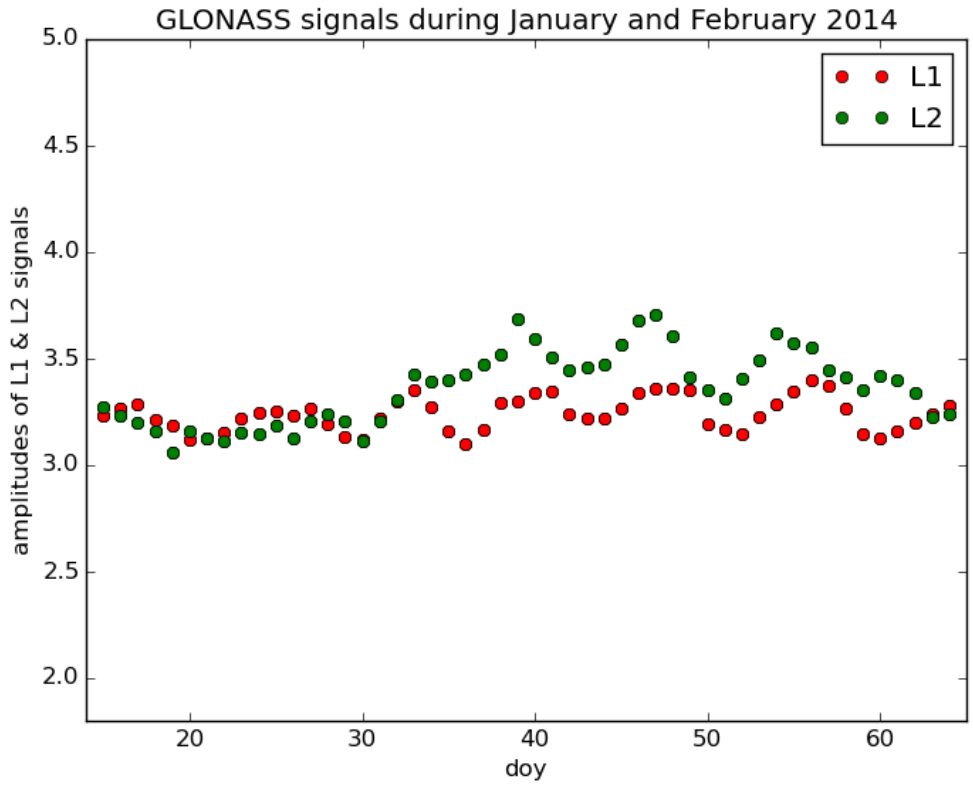

Figure 4.12: Amplitudes of GLONASS L1 and L2 multi-path signals

Next, in figure 4.13 one can see the damping factors of the GLONASS satellite signals. We see that they followed, roughly, the same distribution as the damping factors of the GPS signals. The L1 signals varied between 50 and 56 units, whilst the L2 signals between 50 and 60 units approximately.

If we compare, now, the above figure with the figure 4.7, we will see that for L1 signals, the damping factor for the non-ice period, varied from 50 to 56 units, while for L2 signals this variation was from 56 to approximately 70. Thus, we can observe that the damping factors coincide with the values for which the sea surface was not frozen.

Finally, in the Appendix the reader can find a figure (Figure .13) with the temperature variation during January - February 2014.

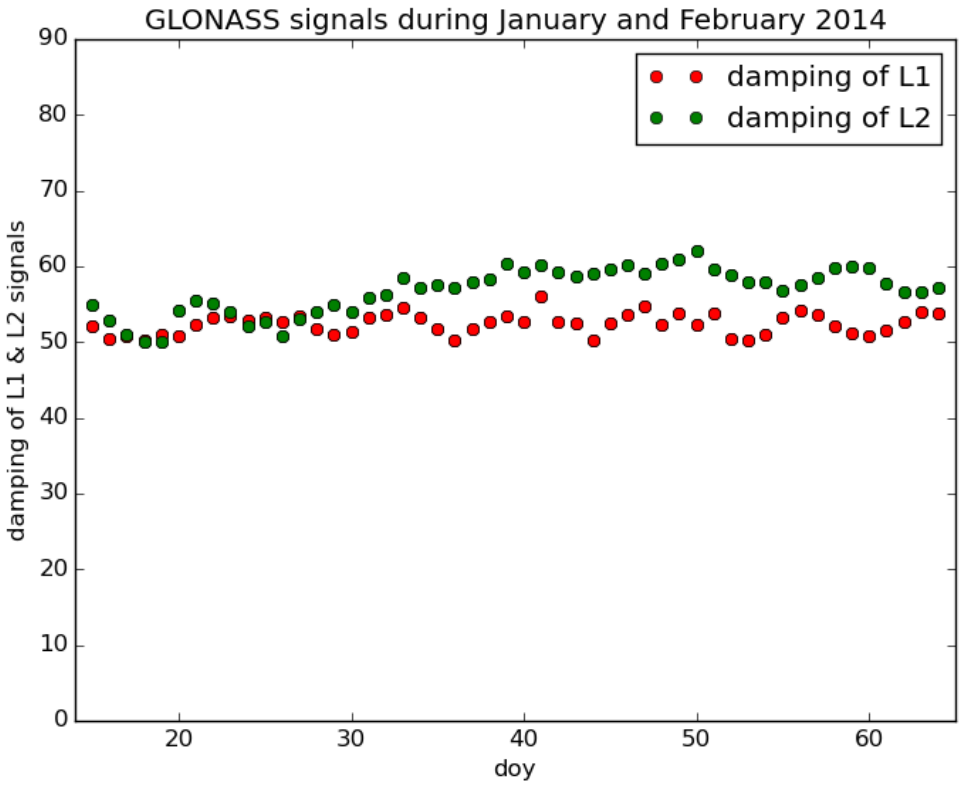

Figure 4.13: Damping factors of GLONASS L1 and L2 multi-path signals

4.3.2 July - August 2013 (doy 197 - doy 229)

The objective purpose behind these measurements during July and August was to be able to compare our initial results (for the ice case) to results during the summer period, where we could easily spot the differences both in the amplitudes and damping factors. Since the temperature in Onsala was high during the summer, as one can see in the Appendix A in figure .14, one could, logically, expect that the amplitudes of the GPS signals during this period would be low (since the sea would not be frozen). In the following figure (Figure 4.14) we can see that the amplitudes of L1 and L2 signals were almost identical and varied between 3.1 to 3.6. Moreover, there is no steep change in their values. Again, if we take a look at figures 4.4 and 4.8 we will observe that the maximum values of the GPS amplitudes for those cases (sea-ice surface) varied from 4 to 4.5 approximately, while the lowest values were almost at the level of 3 for the January-February 2013 case and slightly larger than 3 for the January-February 2012 case. Moreover, we can see in Figure 4.10 that the amplitudes were almost at the same level as the amplitudes for July-August 2013. This indicates that the temperature does not affect the surface as long as the water is in liquid form. However, these data (July-August 2013 and January-February 2014) were a very good reference point for our measurements for the ice-case.

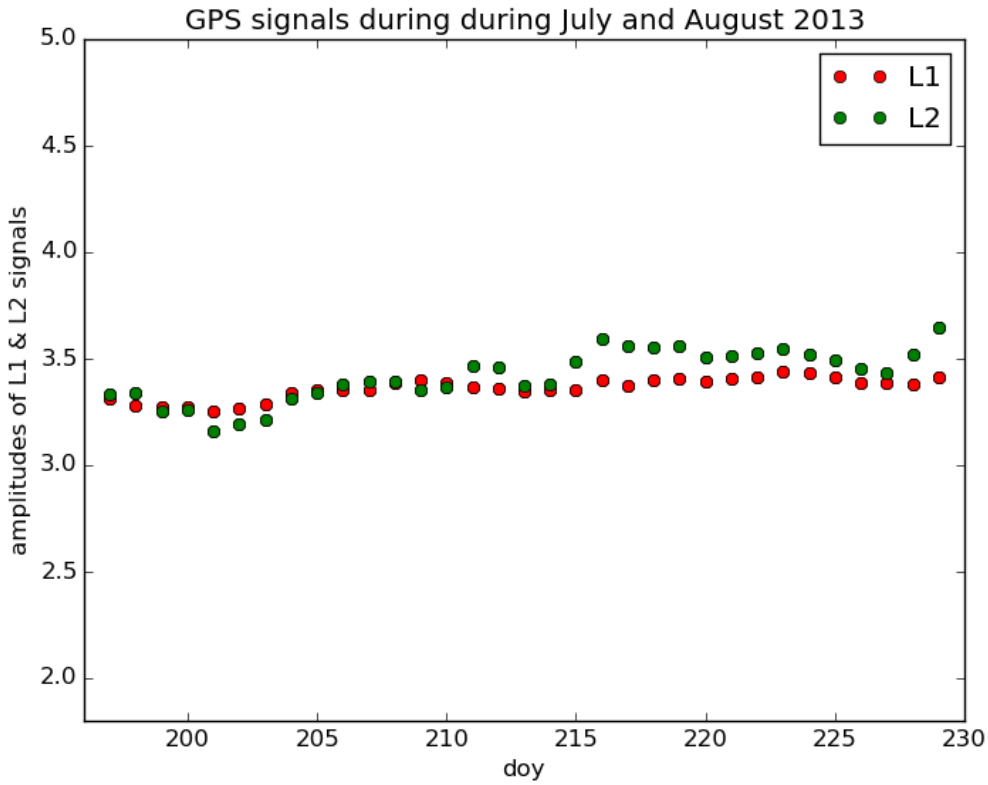

Figure 4.14: Amplitudes of GPS L1 and L2 multi-path signals

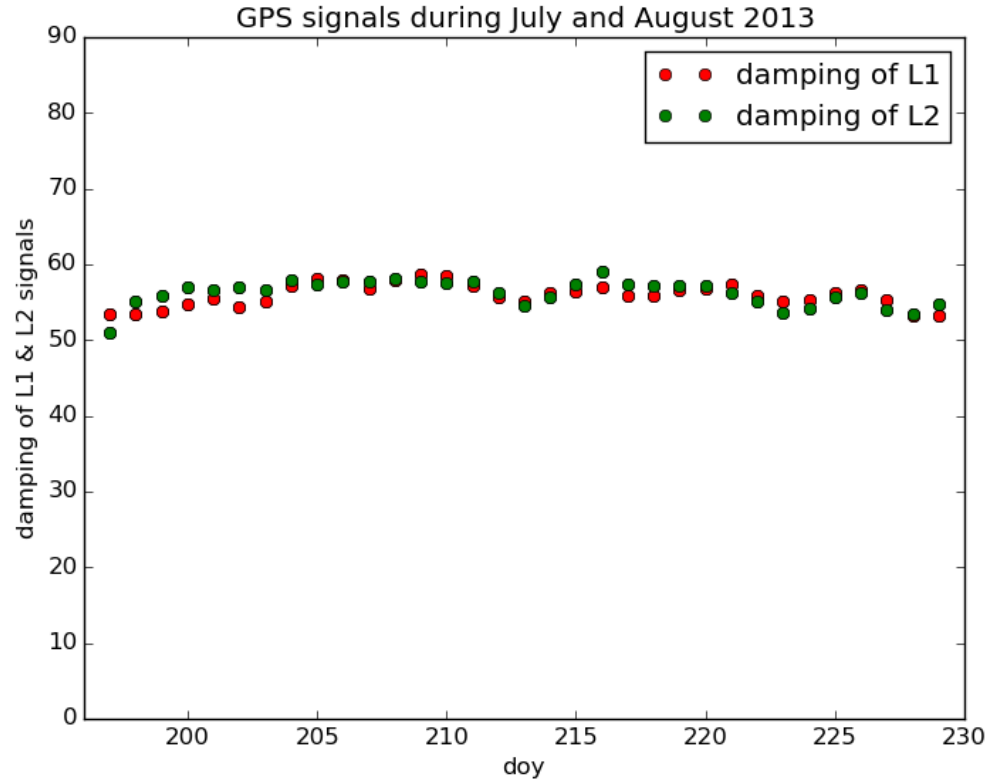

Figure 4.15: Damping factors of GPS L1 and L2 multi-path signals

In the above figure (Figure 4.15) we can see the damping factors for this period. As one would expect, the dampings have large values that vary from 50-60 approximately. During this period there is no ice in Onsala. If we compare, now, these results with the ones in the figure 4.11 we will observe that the variation is almost the same in the damping both for L1 and L2 multi-path signals. By taking a look at figures 4.5 and 4.9, that show the two cases when ice was observed, we can see that the minimum value of the damping factors of L1 and L2 interference signals (with ice present) was 20, while the maximum was 60 (when ice had melted) both for January-February 2012 and January-February 2013.

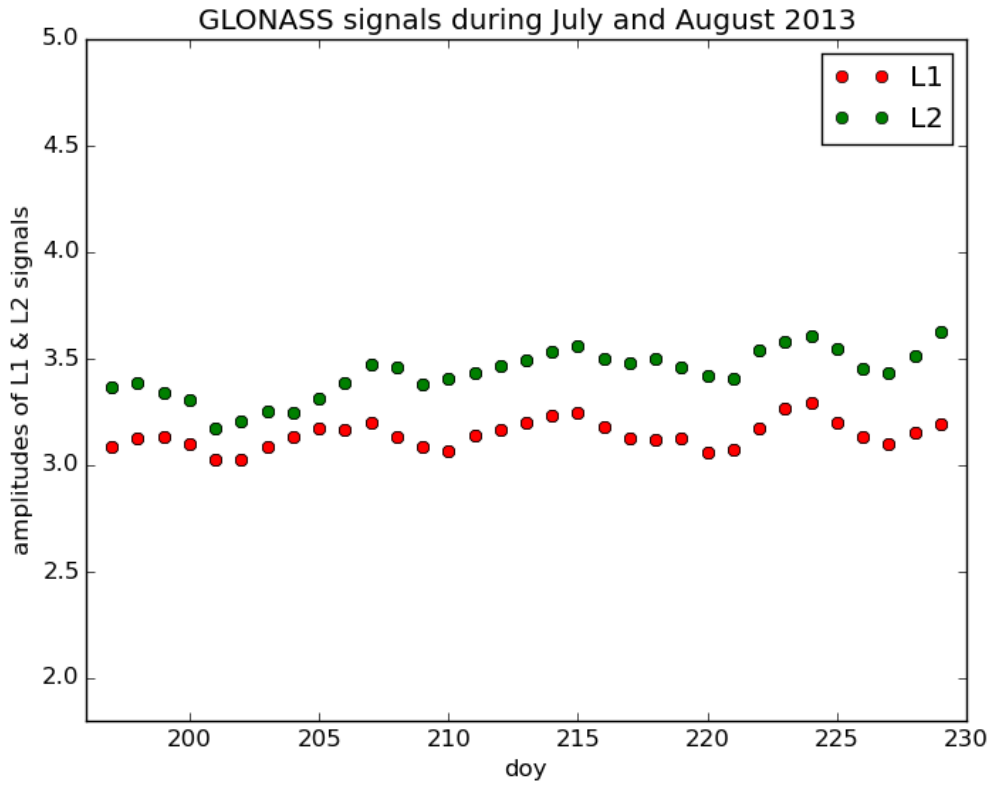

Figure 4.16: Amplitudes of GLONASS L1 and L2 multi-path signals

Figure 4.16 shows the amplitudes of the GLONASS L1 and L2 signals for the same period of time. The amplitudes follow the same distribution as the GPS signals. Again, we see no steep changes, which might indicate a change in the sea surface. By taking a look at figure 4.12, one can see that the amplitudes followed an approximately same distribution as in the case of the GLONASS multi-path signals for July-August 2013. We can see that their values are below 3.5 for the L1 signals and below 4 for the L2 signals, when in the sea-ice case (January-February 2012), in figure 4.6, the values of the amplitudes are above 4 for the GLONASS L1 signals and above 4.5 for the GLONASS L2 signals.

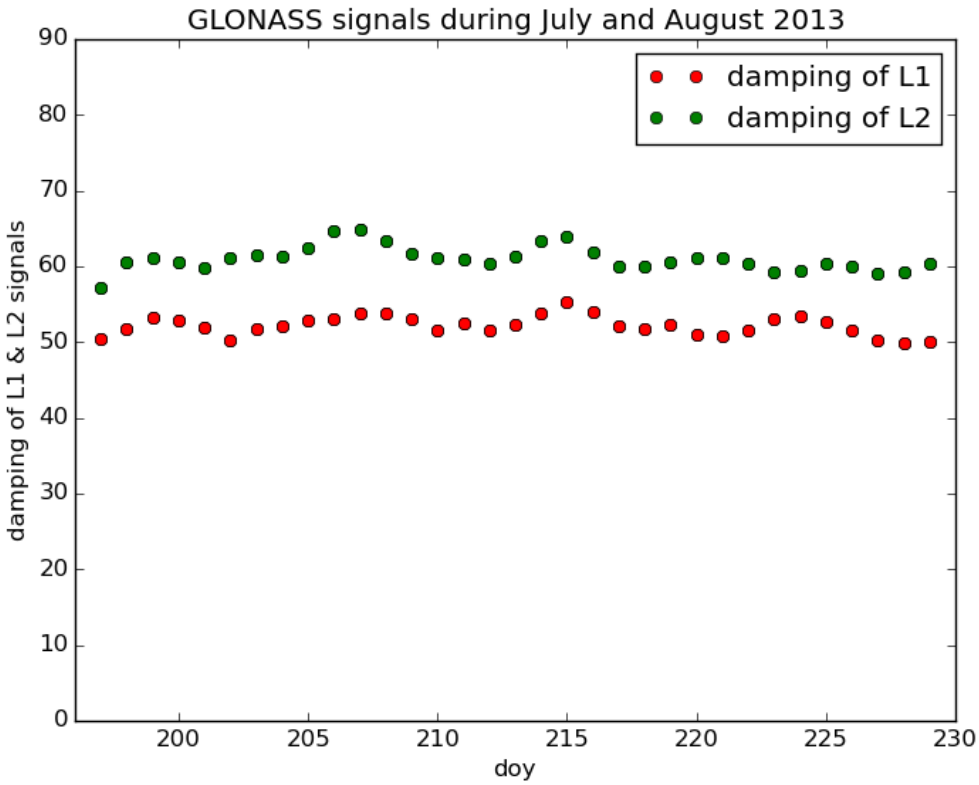

Figure 4.17: Damping factors of GLONASS L1 and L2 multi-path signals

Figure 4.17 shows the damping factors' distribution of the GLONASS L1 and L2 signals. We, again, observe that their values were large enough and coincide with the GPS values for the same period of time, as can be seen in figure 4.15. Comparing now these values with the ones observed for January-February 2014, in figure 4.13, one can see that the values coincide and varied between 50 and 60 for L1 and L2 interference signals. At the same time, by looking at figure 4.7 one can easily observe that the values of the damping factors that indicated a sea-ice surface were much lower than the ones we observed for January-February 2014 and July-August 2013.

4.3.3 March - April 2015 (doy 60 - doy 91)

This subsection is the last of Section 4.3 that analysed data which do not indicate sea-ice conditions and concerns data collected during the period of March and April 2015. Unfortunately, for this specific period of time we had only GPS data available.

In figure 4.18 one can observe mainly two things. Firstly, that there was a shift in the amplitude values during doy 67 - doy 69, which, however, should not worry us that much, since it had, probably, to do with some noise error in the receiver and secondly, one can see that the amplitudes followed a similar distribution as in the previous cases of section 4.3, where there was no ice in Onsala. The temperature during this period can be found in the Appendix, in figure (.15).

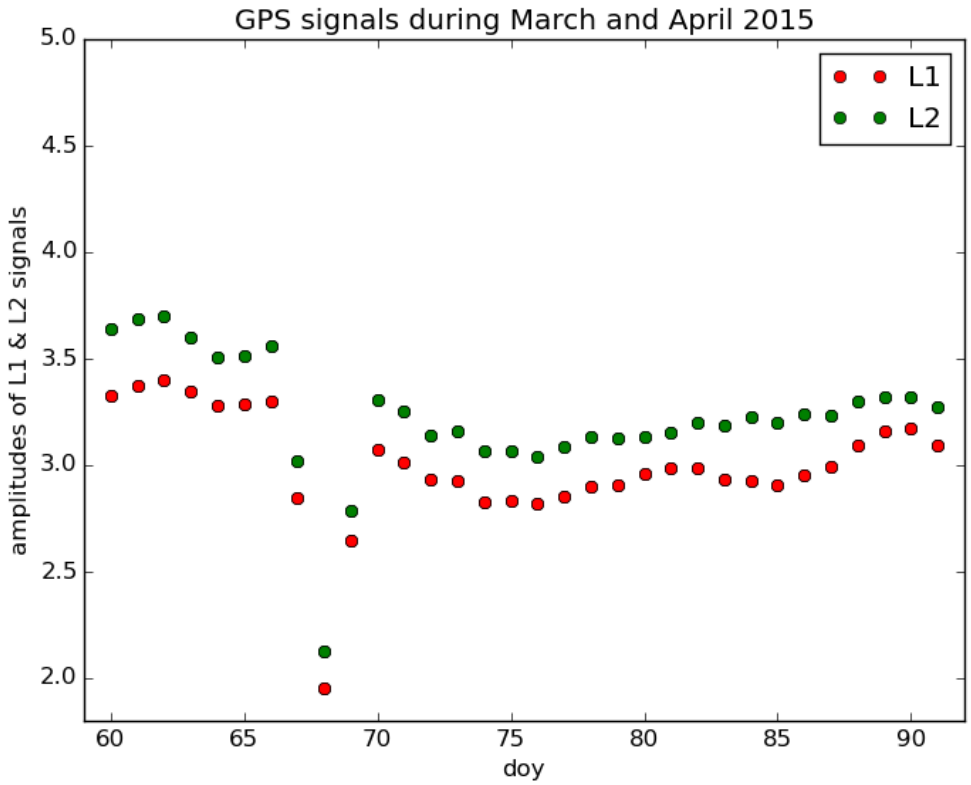

Figure 4.18: Amplitudes of GPS L1 and L2 multi-path signals

We can, therefore, claim that during March and April 2015 there was no ice in the sea in Onsala as there was no ice either during July and August 2013 and January and February 2014.

The last figure (Figure 4.19) shows the damping factors of GPS L1 and L2 multi-path signals. As expected, their values were large enough to be able to claim that there was no ice during this time of period. The values of L1 signals were approximately 60 and the ones for L2 signals were approximately 45.

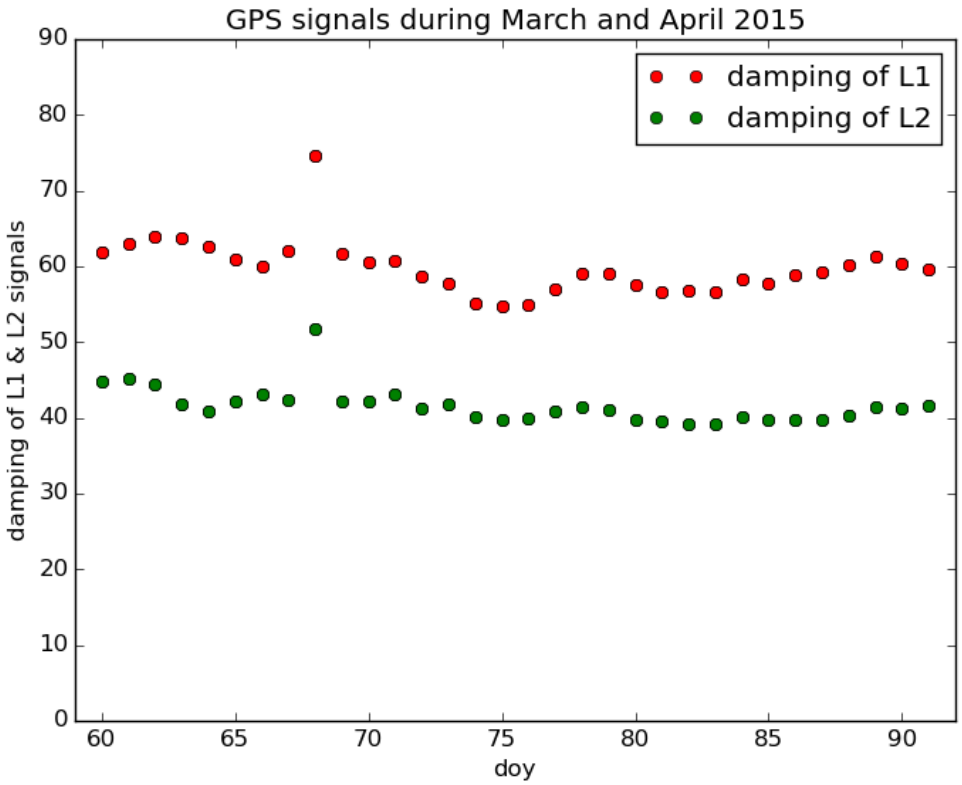

Figure 4.19: Damping factors of GPS L1 and L2 multi-path signals

Chapter 5

Conclusions and Future Work

In this Chapter, we compared all the collected data that indicated ice on the sea surface and tried to create a model, which could be used in a more general way in the near future and could be applied to various GNSS sites around the world. We also showed what the level of correlation between the temperature and damping factor was and what this indicates about their relation. The last section describes the future work that can be done in order for our observations to be further improved.

5.1 Quantitative model

As described above, we tried to quantitatively model our results so that they can be applied to various GNSS sites around the world. In order to achieve this, we examined figures 4.5, 4.7 and 4.9 both for L1 and L2 multi-path signals. We separated the L1 and L2 damping distributions into 3 sections: no-ice period, ice period, no-ice period. For all these sections, we calculated a mean value of the damping and added also a safety margin of 3 *sigma*, where *sigma* is the standard deviation of L1 and L2 multi-path signals averaged again, since it was different for the ice period and the no-ice period. The purpose of this procedure was to be able to see clearly how much the damping decreased during our observations. The above procedure was applied only to the data where we had sea-ice in Onsala, since there was no reason for applying it to data with no sea-ice results. Those data had the same damping during our observations.

The first figure that was produced was the one for GPS L1 multi-path signals during January - February 2012 (doy 15 - doy 64) and can be seen in figure 5.1. There, we can see that the average damping from doy 15 to doy 31 was calculated to be approximately 58 units. This period represents a period when the sea was not frozen (one can also refer to figure 4.5). After a transition period of 3 days where ice started to be accumulated, we ended up in a damping of 23 units for doy 34 to doy 43. During those days, the sea in Onsala was frozen. As one can deduce from the figure, the decrease in the damping was 60%. After that, there is another transition period of 10 days, now, when the ice started to melt and we ended up again to a non-ice period during doy 53 and doy 64, when the ice melted and the sea was not frozen.

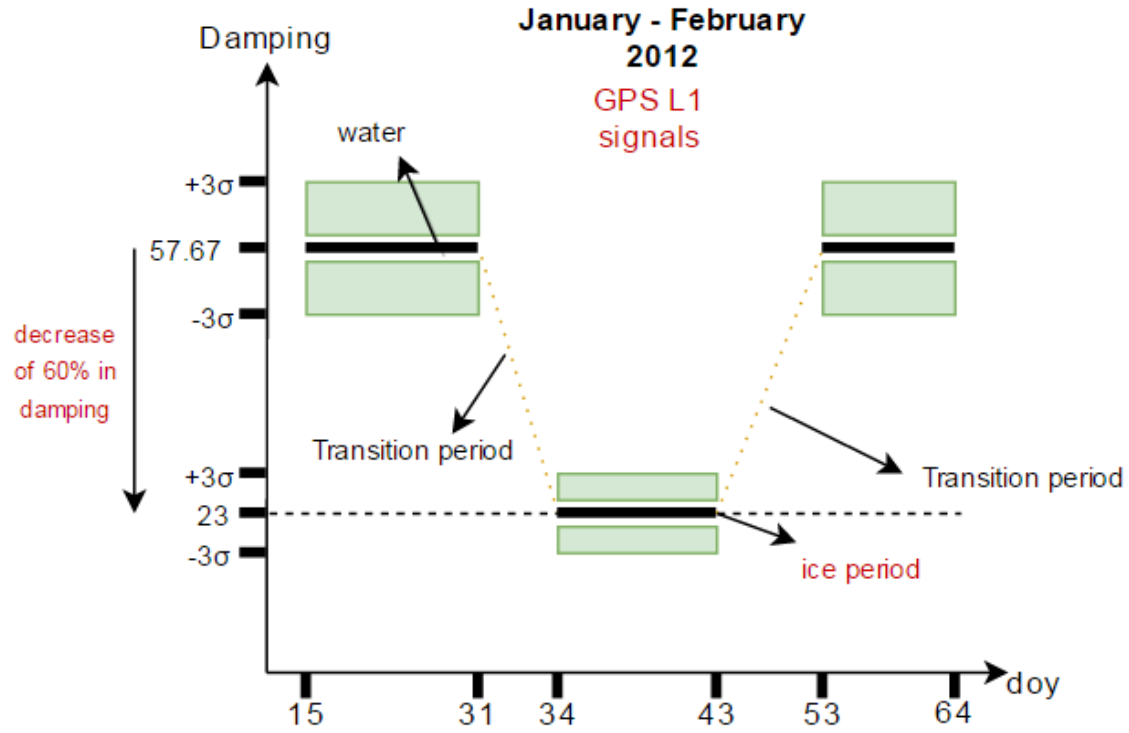

Figure 5.1: January-February 2012 GPS L1 multi-path signals

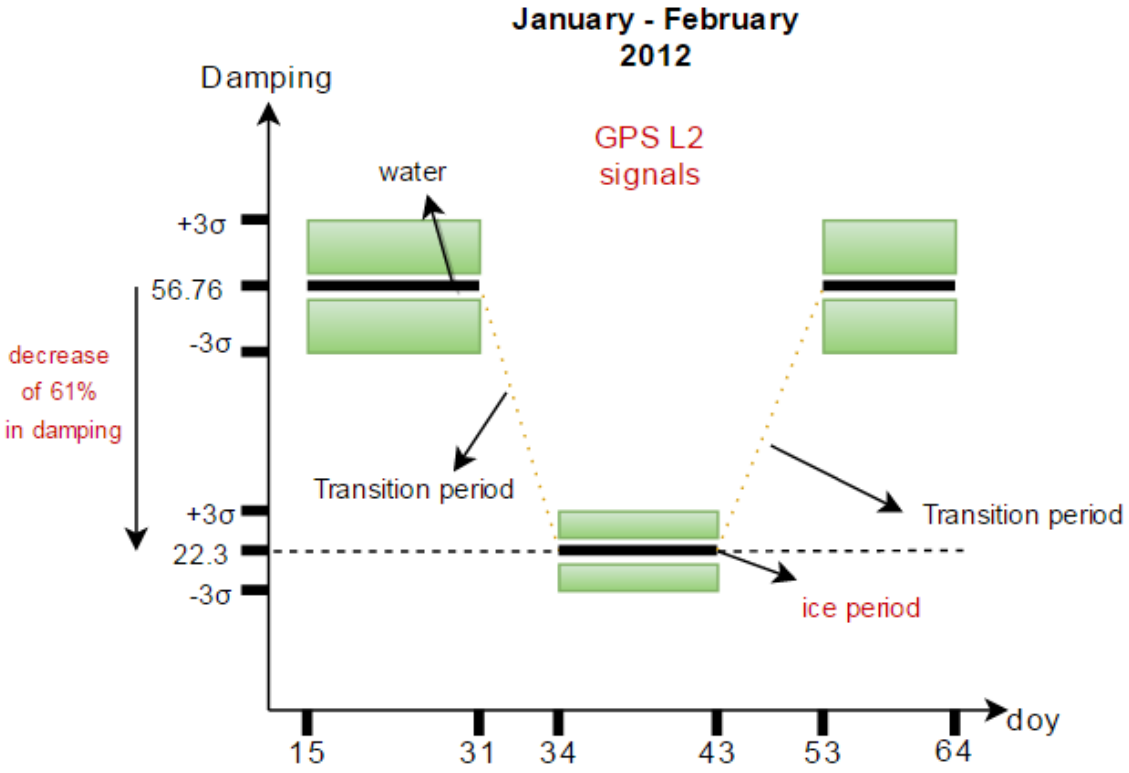

Figure 5.2: January-February 2012 GPS L2 multi-path signals

The same procedure was followed for the GPS L2 multi-path signals. As can be seen from the above figure (Figure 5.2) the average value of the damping factor during the non-ice or "water" period was approximately 57 units and lasted from doy 15 to doy 31. Then, after the transition period, when the ice started to be accumulated, the value of the damping dropped to 22.3 units for 9 consecutive days (doy 34 - doy 43). As the reader can see, the decrease in the damping was 61%. After these 9 days, we can see a transition period of 10 days when the ice started to melt and then the damping factor's level returned to its initial value of almost 57.

Next, we examined the GLONASS multi-path signals. In the following figure (Figure 5.3) we can see the decrease in the damping of the GLONASS L1 interference signals.

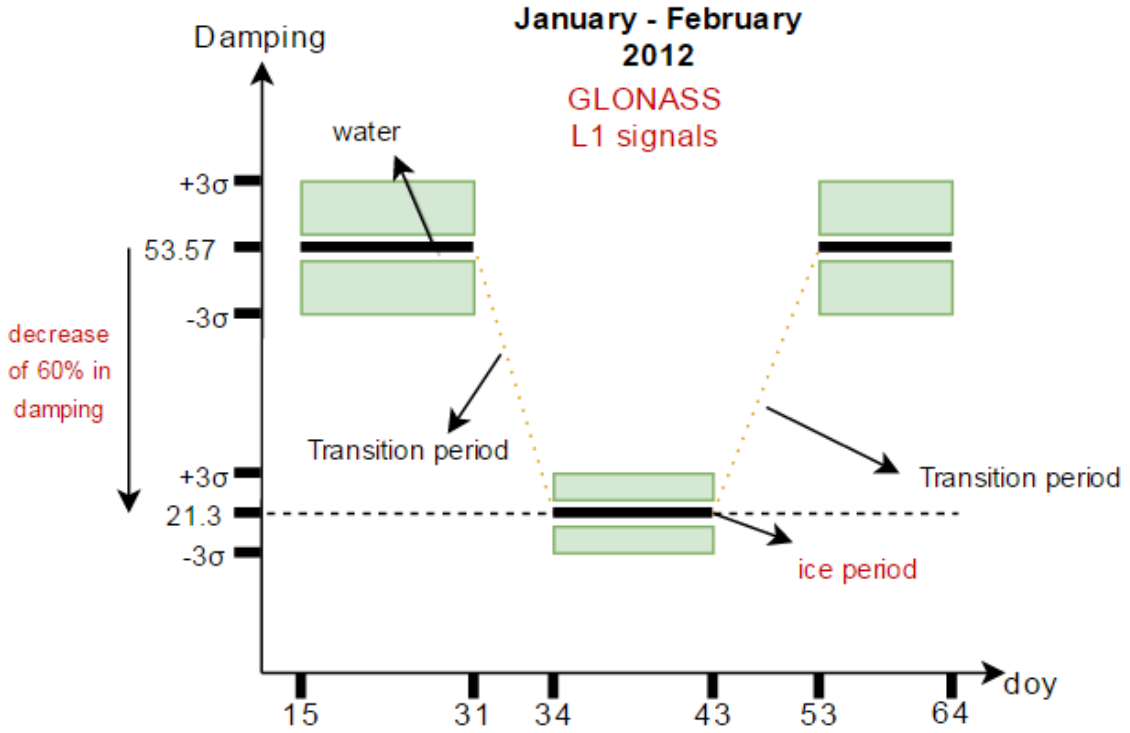

Figure 5.3: January-February 2012 GLONASS L1 multi-path signals

Again, the same procedure was followed and the same results were observed. The mean value of the damping, during the first non-ice period during doy 15 to doy 31, was calculated to be approximately 54. After the transition period that lasted 3 days, the value of the damping was found to be 21.3, that is we had a decrease of 60%. This situation continued for 9 days. Then, another transition period and the damping value was 54 again. We can see that the results of the GLONASS L1 signals coincide with the ones for the GPS L1 signals.

The January - February 2012 period ends with the examination of the GLONASS L2 multi-path signals. The results can be seen in figure 5.4. The average values of the damping for the GLONASS L2 signals was approximately 64 units. Then, we had, again, a transition period of 3 days until doy 34, when the damping dropped to roughly 25 units, which was a decrease of 61%. The damping returned to its former

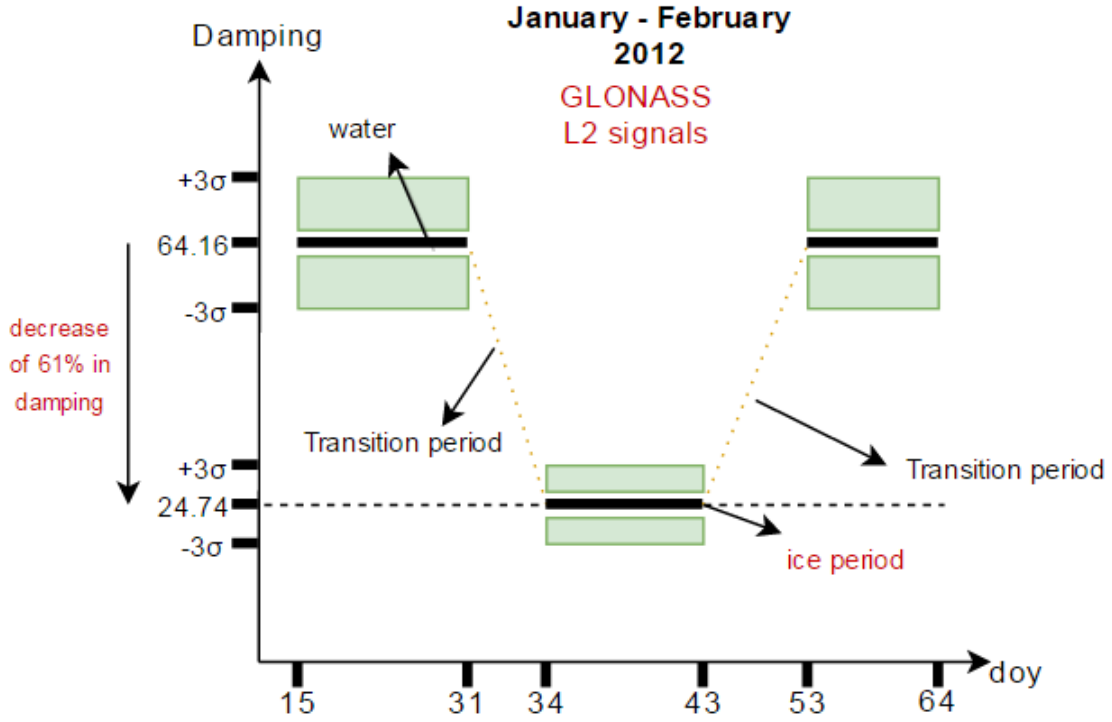

Figure 5.4: January-February 2012 GLONASS L2 multi-path signals

value at doy 53. We, again, see that the decrease in the damping for the GLONASS L2 multi-path signals coincides with the decrease of the GPS L2 multi-path signals.

Results during January - February 2013 are presented next. As was mentioned in section 4.2.2, only GPS data were available. Therefore, only figures for GPS L1 and L2 multi-path signals are presented. In figure 5.5 we can see a non-ice period during doy 15 to doy 18, where the damping was approximately 55 and after a transition period of 3 days, its value was reduced to roughly 25 units. This decrease reflected to a 55% in the damping. After 7 days of sea-ice conditions, there was a transition period of 9 days after which the damping returned to its initial value of 55 in doy 37.

As for the GPS L2 interference signals, they can be seen in figure 5.6. The initial mean value of the damping during doy 15 and doy 18, when no ice was observed, was roughly 56. Then, after a transition period of 3 days, this value dropped to approximately 26. This was the period when ice was present in the area of the GNSS tide gauge in Onsala. The decrease in the damping was 53.8% for the GPS L2 signals. Then, again, after the transition period, the damping returned to its initial value.

After having examined the results during January - February 2012 and 2013, where we had ice in Onsala, we can conclude that this model can me applied to any GNSS tide gauge around the globe and can be, therefore, tested and see if it is efective. The reference point of whether there was ice or not is going to be the decrease in the damping of the signals in each site and must be at least a decrease of 50%.

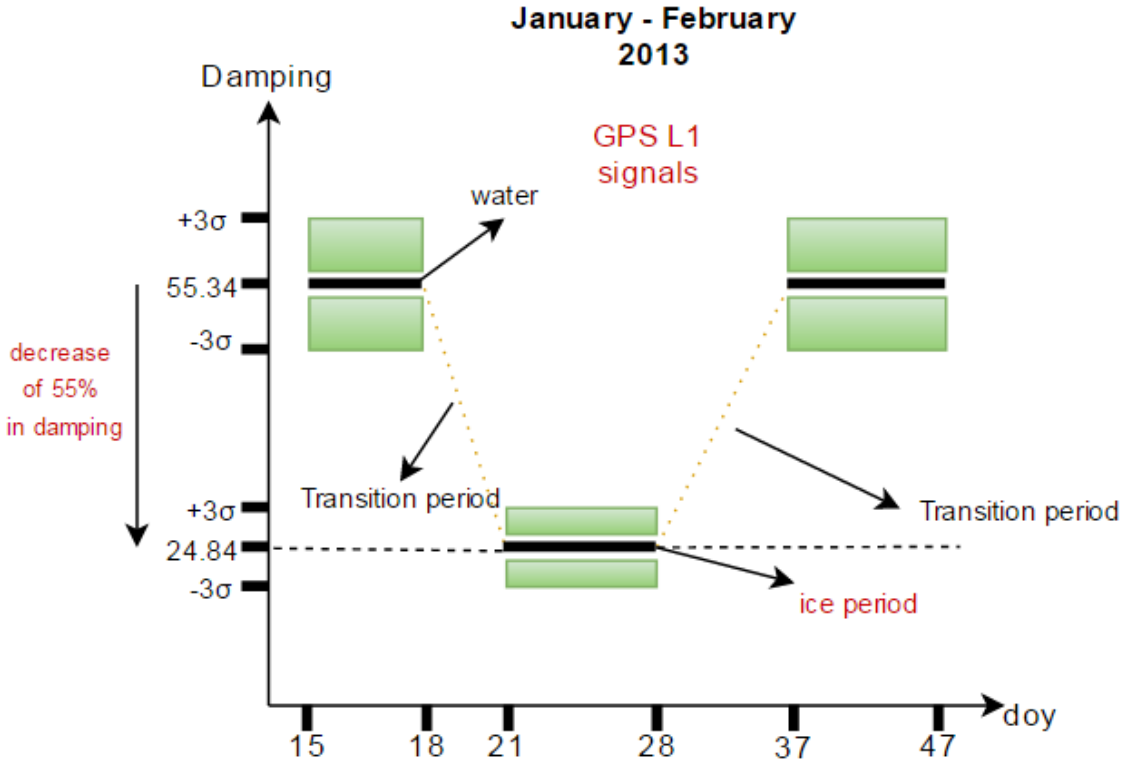

Figure 5.5: January-February 2013 L1 multi-path signals

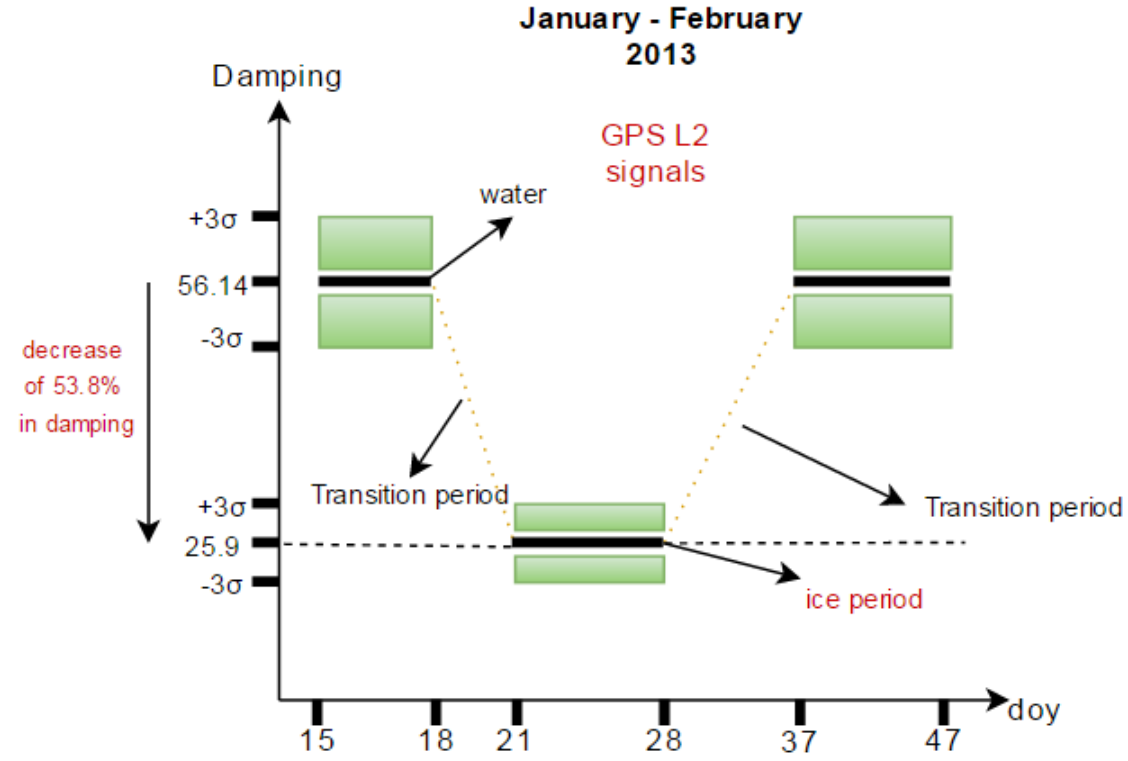

Figure 5.6: January-February 2013 L2 multi-path signals

5.2 Temperature and Damping correlation

As was discussed in Chapter 4 the temperature does not have a linear relation with the damping. This means that if the temperature decreases, this does not necessarily mean that the damping will decrease also (at least not immediately). In the following figures, we calculated the Pearson correlation coefficient between the temperature and the damping for both GPS and GLONASS signals during January - February 2012 and GPS signals during January - February 2013.

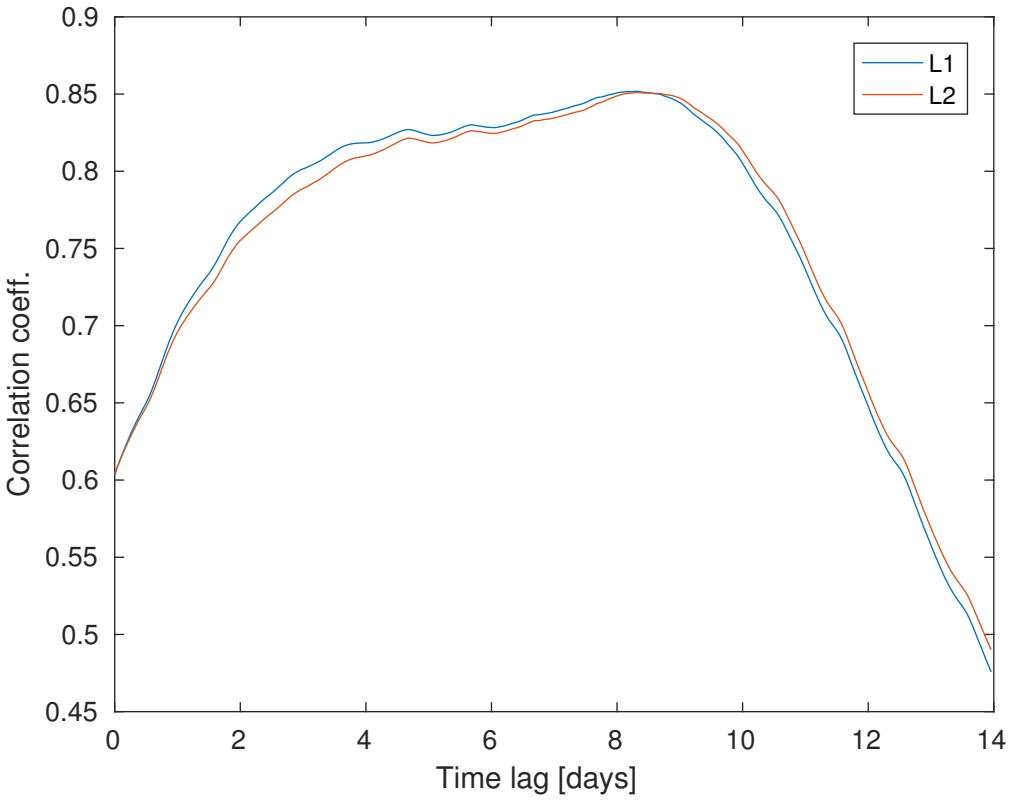

Figure 5.7: Temperature and GPS L1 and L2 damping correlation during January-February 2012

In the above figure (Figure 5.7) we can see the correlation between the temperature and the damping for L1 and L2 GPS signals. As we can observe, the correlation coefficient increases gradually and takes its maximum value after approximately 9 days. This means that after the temperature started decreasing, it took 9 days for the water to freeze and consequently the damping factor to decrease. Another important observation is that the correlation coefficient increases gradually due to the fact that the ice started to be formed with direction from the bedrock to the sea. This makes sense, if we take into account the fact that the place in Onsala, where the GNSS tide gauge is placed, is a bay with all the geographic characteristics and singularities of a bay, as can be seen in figure 4.1.

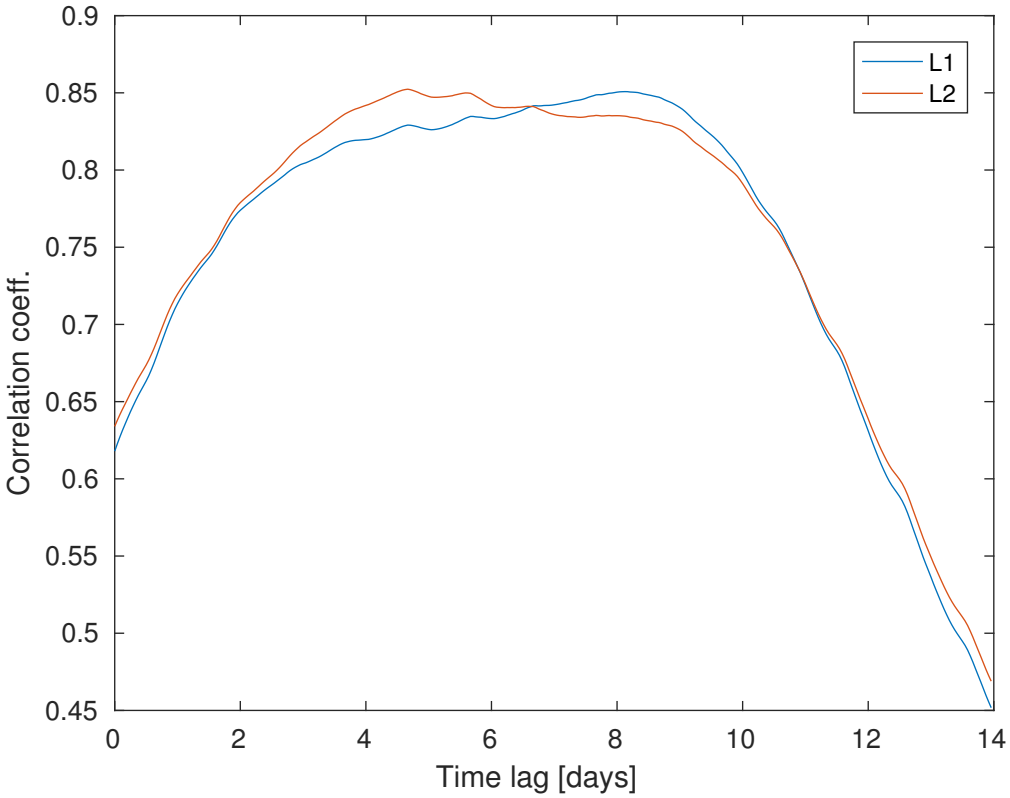

Figure 5.8: Temperature and GLONASS L1 and L2 damping correlation during January-February 2012

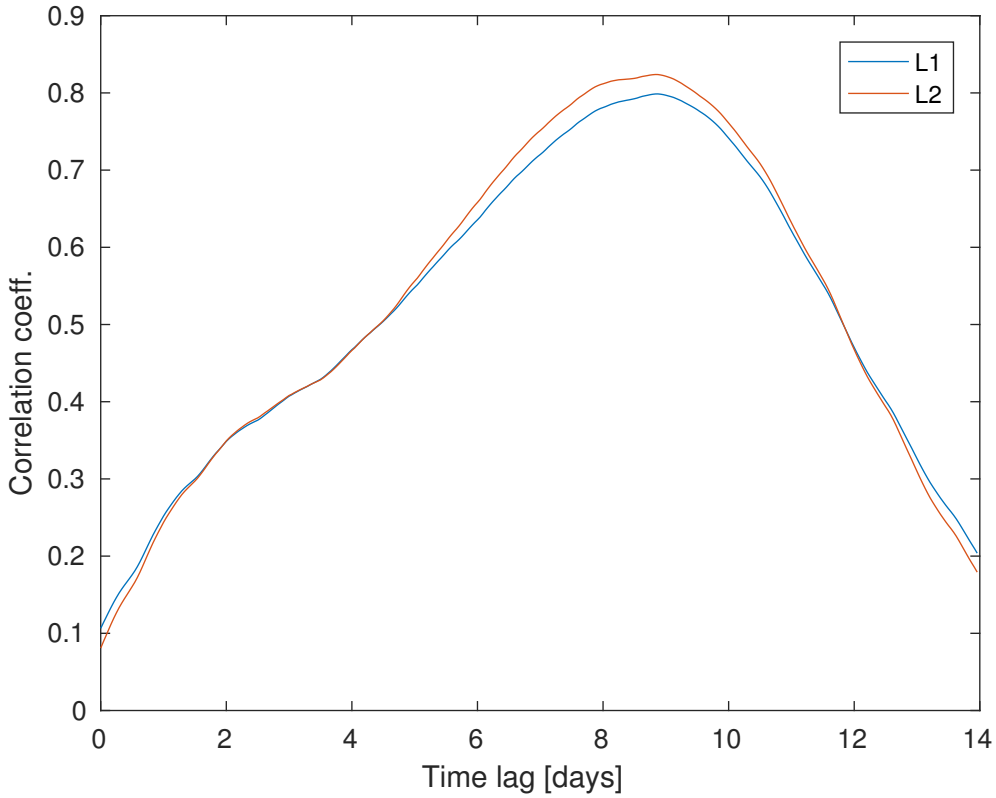

Figure 5.9: Temperature and GPS L1 and L2 damping correlation during January-February 2013

In figure 5.8 one can observe the correlation coefficient of L1 and L2 GLONASS signals. For the L2 signal, there seems to be a less pronounced peak for a time lag of 9 days, but for the L1 signal we can see that the correlation coefficient is at its maximum value after approximately 9 days, as it was for the GPS L1 signal.

In figure 5.9 the reader can see that, again, after roughly 9 days the sea got frozen after the temperature had dropped. This applies both for L1 and L2 signals.

To sum up, we saw that the temperature definitely influences the sea surface and consequently the damping, but it takes a considerable amount of time before this to happen.

5.3 Future Work

Our measurements were fairly accurate, since we took advantage of both GPS and GLONASS signals, but they can become even more accurate in the future when Galileo becomes operational. Then the combination of the three systems will increase the number of the observations and hence the temporal resolution of the SNR analysis that we followed in this thesis. Taking advantage of multi-GNSS observations will also increase the spatial resolution (better sea surface coverage per time unit). Another important parameter is the C/A code modulated on $L2_C$ carrier, which can, also, be used, instead of the P(Y) code for the GPS L2 signals, if more satellites become capable of using this frequency. $L2_C$ signal can lead to greater data recovery than the L2 signal.

Another factor that could contribute to the results and especially the comparison between them is the bubbler tide gauge that is installed in Onsala and unfortunately was not available due to some practical problems during the observations.

Last, but not least, this model could be used to various coastal GNSS sites around the world in order to compare their results and then if it is found to be effective, a database of ice and/or snow data in those stations could be created.

Bibliography

[1] Surendra Adhikari and Erik R Ivins. Climate-driven polar motion: 2003–2015. *Science Advances*, 2(4):e1501693, 2016

[2] Felipe G. Nievinski and Kristine M. Larson. Forward modeling of gps multipath for near-surface reflectometry and positioning applications. *GPS Solutions*, 18(2): 309–322, 2014. ISSN 1521-1886. doi: 10.1007/s10291-013-0331-y. URL http://dx.doi.org/10.1007/s10291-013-0331-y.

[3] Wikipedia. Effects of global warming — wikipedia, the free encyclopedia, 2016. URL `https://en.wikipedia.org/w/index.php?title=Effects_of_global_warming&oldid=717049213`

[4] Wikipedia. Effects of global warming on humans — wikipedia, the free encyclopedia, 2016. URL `https://en.wikipedia.org/w/index.php?title=Effects_of_global_warming_on_humans&oldid=719123474`

[5] Thomas J Doherty and Susan Clayton. The psychological impacts of global climate change. *American Psychologist*, 66(4):265, 2011

[6] M Martin-Neira. A passive reflectometry and interferometry system (paris): Application to ocean altimetry. *ESA journal*, 17:331–355, 1993

[7] James L Garrison and Stephen J Katzberg. The application of reflected gps signals to ocean remote sensing. *Remote Sensing of Environment*, 73(2):175–187, 2000

[8] S. Gleason, S. Hodgart, Yiping Sun, C. Gommenginger, S. Mackin, M. Adjrad, and M. Unwin. Detection and processing of bistatically reflected gps signals from low earth orbit for the purpose of ocean remote sensing. *IEEE Transactions on Geoscience and Remote Sensing*, 43(6):1229–1241, June 2005. ISSN 0196-2892. doi: 10.1109/TGRS.2005.845643.

[9] Bernhard Hofmann-Wellenhof, Herbert Lichtenegger, and James Collins. *Global positioning system: theory and practice*. Springer Science & Business Media, 2012

[10] Gérard Maral and Michel Bousquet. *Satellite communications systems: systems, techniques and technology.* John Wiley & Sons, 2011

[11] Navipedia. Tropospheric delay — navipedia, 2013. URL `http://www.navipedia.net/index.php?title=Tropospheric_Delay&oldid=12152`

[12] Navipedia. Ionospheric delay — navipedia„ 2016. URL `http://www.navipedia.net/index.php?title=Ionospheric_Delay&oldid=13741`

[13] Günter Seeber. *Satellite geodesy: foundations, methods, and applications.* Walter de Gruyter, 2003

[14] International GNSS Service. About igs. URL `http://http://www.igs.org/about`

[15] Wikipedia. Global positioning system — wikipedia, the free encyclopedia, 2016. URL `https://en.wikipedia.org/w/index.php?title=Global_Positioning_System&oldid=72537970`

[16] Wikipedia. Glonass — wikipedia, the free encyclopedia, 2016. URL `https://en.wikipedia.org/w/index.php?title=GLONASS&oldid=725298418`

[17] Johan Löfgren. *Local Sea Level Observations Using Reflected GNSS Signals.* Doktorsavhandlingar vid Chalmers tekniska hgskola. Ny serie, no: 3637. Department of Earth and Space Sciences, Space Geodesy and Geodynamics, Chalmers University of Technology„ 2014. ISBN 978-91-7385-955-4. 62

[18] ESA. First results, 2014. URL `http://www.esa.int/Our_Activities/Navigation/Galileo/First_results`

[19] ESA. What is galileo, 2015. URL `http://www.esa.int/Our_Activities/Navigation/Galileo/What_is_Galileo`

[20] ESA. Facts and figures, 2014. URL `http://www.esa.int/Our_Activities/Navigation/Facts_and_figures`

[21] Navipedia. Galileo signal plan — navipedia„ 2014. URL `http://www.navipedia.net/index.php?title=Galileo_Signal_Plan&oldid=12522`

[22] Wikipedia. Beidou navigation satellite system — wikipedia, the free encyclopedia, 2016. URL `https://en.wikipedia.org/w/index.php?title=BeiDou_Navigation_Satellite_System&oldid=725051685`

[23] Cao Chong. Status of compass/beidou development. *In Proceedings of the PNT Challenges and Opportunities Symposium*, 2009

[24] Indian Space Research Organisation. Indian regional navigation satellite system (irnss): Navic, . URL `http://www.isro.gov.in/irnss-programme`

[25] Indian Space Research Organisation. Irnss-1a, . URL `http://www.sac.gov.in/SACSITE/IRNSS-1A.html`

[26] Indian Space Research Organisation. Towards self reliance in navigation-irnss, . URL `http://www.isro.gov.in/irnss-programme/towards-self-reliance-navigation-irnss`

[27] Michael S. Braasch Logan Scott Grard Lachapelle, Mark Petovello. Gnss solutions: Signal acquisition and search, and antenna polarization. *Inside GNSS*, page 2007, 2014

[28] B.R. Rao. *GPS/GNSS Antennas*. GNSS technology and applications series. Artech House, 2013. ISBN 9781596931503. URL `https://books.google.se/books?id=nL-YFWLQrPIC`

[29] Stephen J Katzberg and James L Garrison Jr. Utilizing gps to determine ionospheric delay over the ocean. 1996

[30] Dallas Masters, Penina Axelrad, and Stephen Katzberg. Initial results of land-reflected gps bistatic radar measurements in smex02. *Remote Sensing of Environment*, 92(4):507–520, 2004

[31] H Davies. The reflection of electromagnetic waves from a rough surface. *Proceedings of the IEE-Part IV: Institution Monographs*, 101(7):209–214, 1954

[32] L Bedford, N Brown, and J Walford. *Leica ar25 white paper. Leica Geosystems AG, Heerbrugg, Switzerland*, 2009

[33] Waldemar Kunysz. A three dimensional choke ring ground plane antenna

[34] Aaron Kerkhoff, R Benjamin Harris, Colin P Petersen, and Alex Pickard. Modifications to gps reference station antennas to reduce multipath

[35] Kenneth D Anderson. Determination of water level and tides using interferometric observations of gps signals. *Journal of Atmospheric and Oceanic Technology*, 17(8): 1118–1127, 2000

[36] Kristine M Larson, Eric E Small, Ethan Gutmann, Andria Bilich, Penina Axelrad, and John Braun. Using gps multipath to measure soil moisture fluctuations: initial results. *GPS solutions*, 12(3):173–177, 2008

[37] Kristine M Larson, Ethan D Gutmann, Valery U Zavorotny, John J Braun, Mark W Williams, and Felipe G Nievinski. Can we measure snow depth with gps receivers? *Geophysical Research Letters*, 36(17), 2009

[38] Valery U Zavorotny, Kristine M Larson, John J Braun, Eric E Small, Ethan D Gutmann, and Andria L Bilich. A physical model for gps multipath caused by land reflections: Toward bare soil moisture retrievals. *IEEE Journal of Selected Topics in Applied Earth Observations and Remote Sensing*, 3(1):100–110, 2010

[39] William H Press and George B Rybicki. Fast algorithm for spectral analysis of unevenly sampled data. *The Astrophysical Journal*, 338:277–280, 1989

[40] Kristine M Larson, John J Braun, Eric E Small, Valery U Zavorotny, Ethan D Gutmann, and Andria L Bilich. Gps multipath and its relation to near-surface soil moisture content. *IEEE Journal of Selected Topics in Applied Earth Observations and Remote Sensing*, 3(1):91–99, 2010

[41] Felipe G Nievinski and Kristine M Larson. Inverse modeling of gps multipath for snow depth estimationpart i: Formulation and simulations. *IEEE Transactions on Geoscience and Remote Sensing*, 52(10):6555–6563, 2014

[42] Johan S Löfgren, Rüdiger Haas, and Hans-Georg Scherneck. Sea level time series and ocean tide analysis from multipath signals at five gps sites in different parts of the world. *Journal of Geodynamics*, 80:66–80, 2014

[43] Johan S Löfgren and Rüdiger Haas. Sea level measurements using multi-frequency gps and glonass observations. *EURASIP Journal on Advances in Signal Processing*, 2014(1):1–13, 2014

[44] P. Beckmann and A. Spizzichino. *The Scattering of Electromagnetic Waves From Rough Surfaces*. Pergamon Press, Oxford, U. K, 1963

Appendix

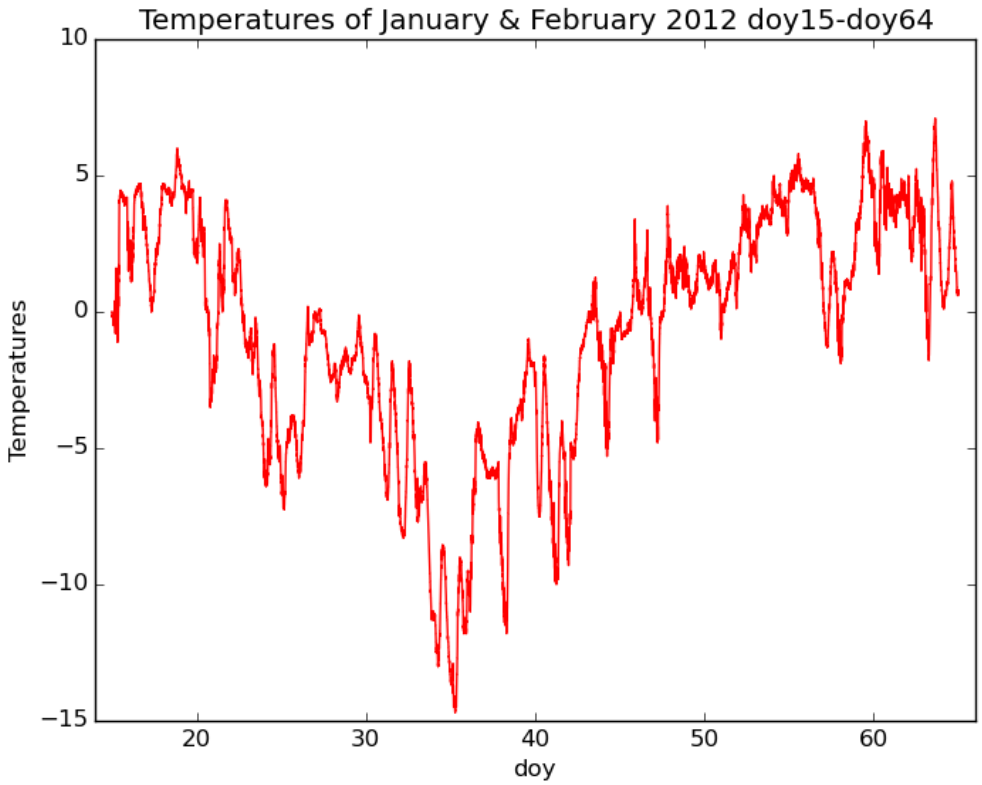

Figure .10: Temperature variation during January - February 2012

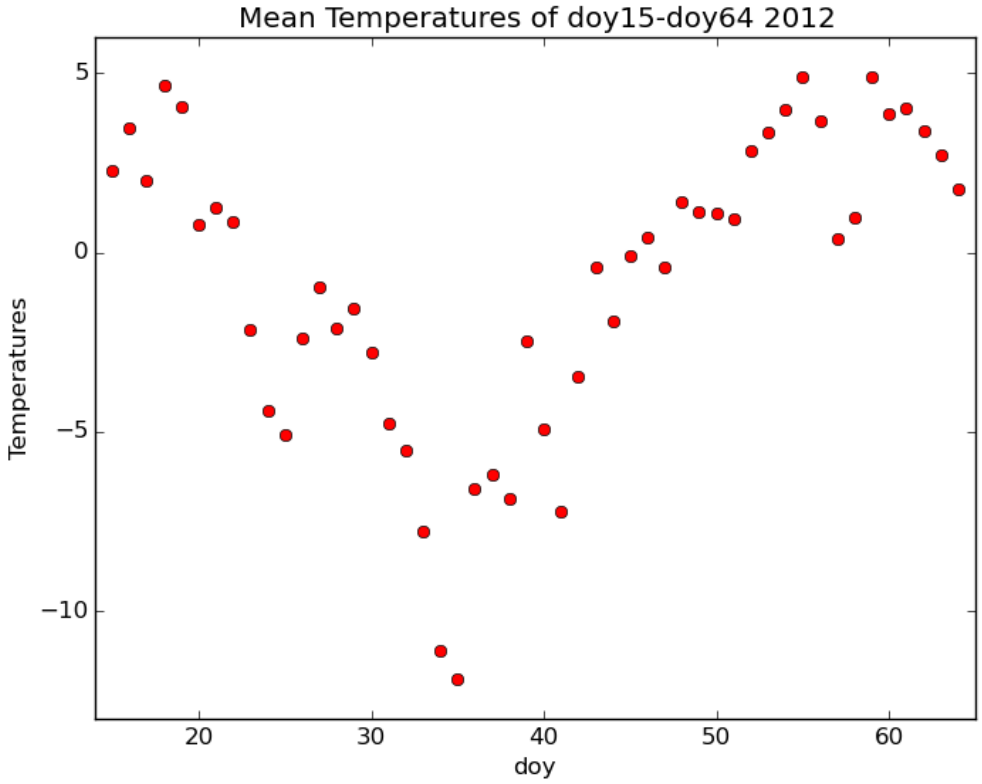

Figure .11: Mean Temperature during January - February 2012

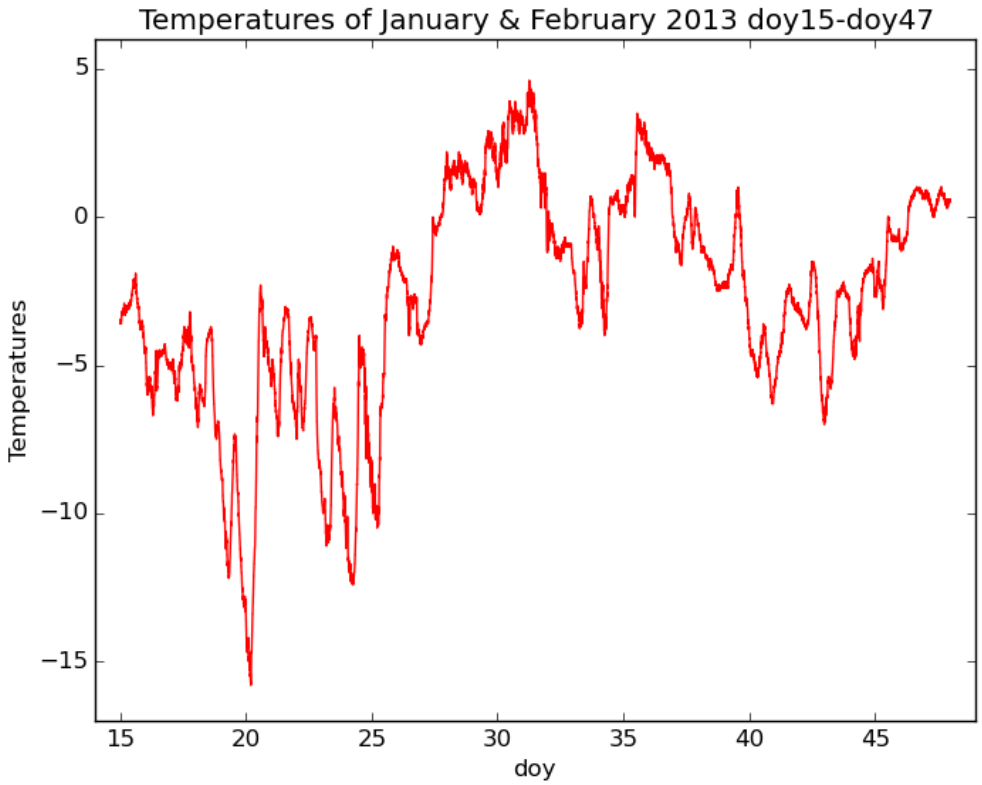

Figure .12: Temperature variation during January - February 2013

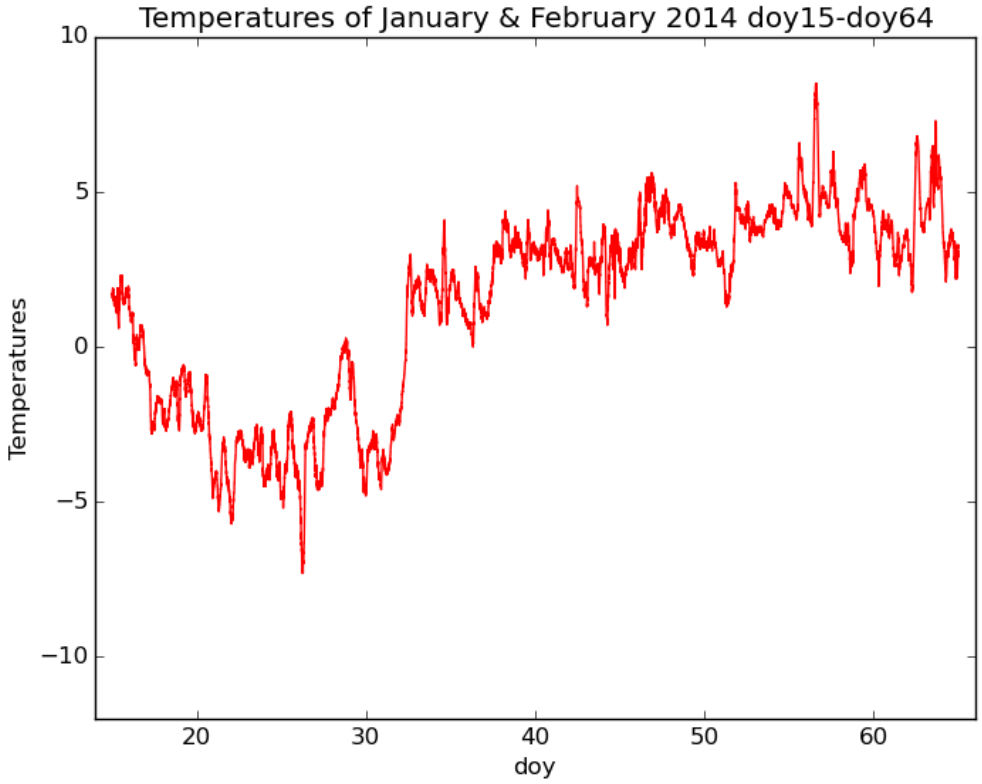

Figure .13: Temperature variation during January - February 2014

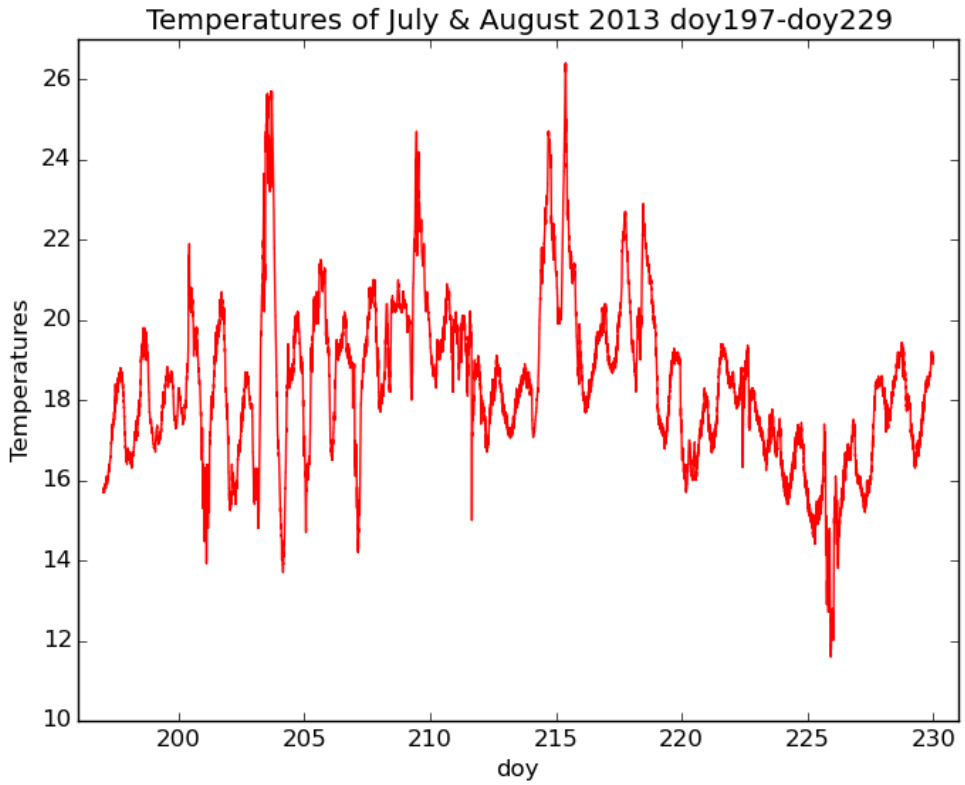

Figure .14: Temperature variation during July - August 2013

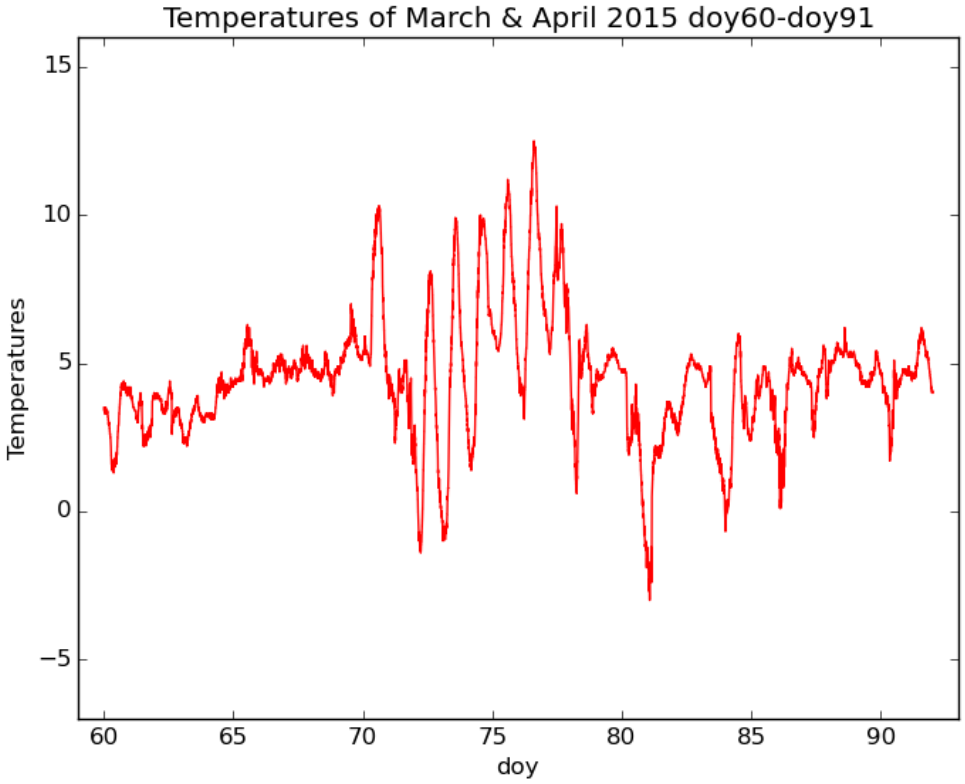

Figure .15: Temperature variation during March - April 2015